Ympäristöministeriö
Miljöministeriet
Ministry of the Environment
ym.fi/puurakentaminen

A Digital end-user toolset for Moisture assessment in Wooden buildings

1st part: Hygro-thermal database (DigiMoist1)

Technical Report (Draft)

Authors: Stefania Fortino, Petr Hradil (VTT)
Reviewers: Tuuli Uimonen (Jartek Invest), Jennifer Enriksson (Stora Enso)

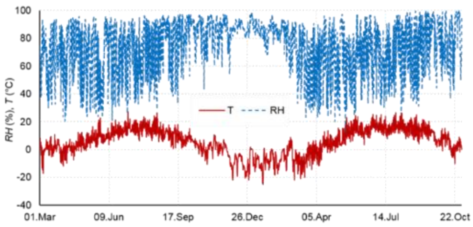

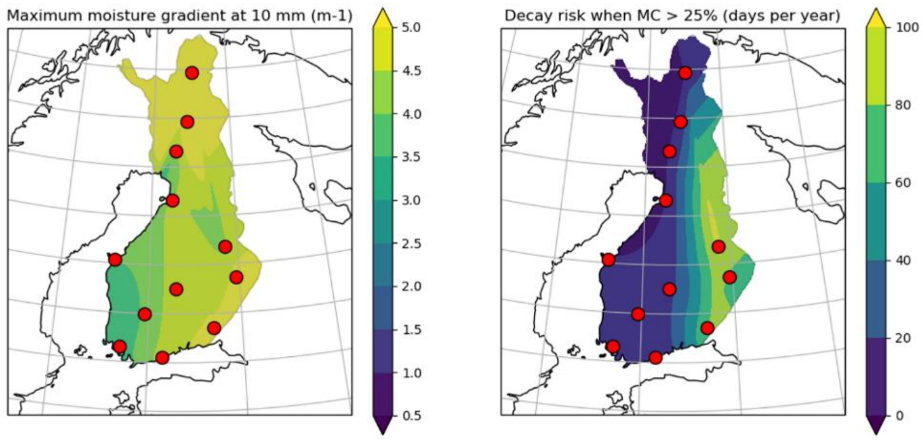

Contents

Summary

The DigiMoist1 project developed an input database as well as a collection of numerical tools, named *DigiMoist toolset*, to simulate the hygro-thermal response of wooden components of buildings under different Finnish climates. The database collects the weather data and the material properties needed to carry out numerical hygro-thermal analyses by using the finite element method (FEM). This allowed performing several pre-calculations to predict the moisture gradients and moisture contents, as well as the related risks of cracking and decay, in various cross sections of wooden components, such as glued laminated timber (glulam) and cross laminated timber (CLT). In addition, experimental tests for measurements of sorption isotherms of Thermowood (TW) were performed and a first model for

moisture transport and decay in untreated and TW decking systems was prepared. The database includes also measurements of scratch resistance in green wood stabilized against water by PEG-impregnation. These have to be considered as references for future measurements of scratch resistance in dry wood and thermowood. All the created tools and the results of the pre-calculations are included in the *DigiMoist toolset* for future implementation in the VTT Modelling Factory web interface to be used as an open source platform for architects, engineers, authorities, industrial companies and students. The project was carried out in collaborations with the DigiMoist1 industrial partners Jartek Invest Oy and Stora Enso, and with some scientific partners of the ForestValue project Click Design in which VTT leads the fourth working package on decay assessment.

1. BACKGROUND ON THE HYGRO-THERMAL MODELLING FOR WOOD

Under outdoor climates, the wooden components are continuously exposed to fluctuations of relative humidity *RH* and temperature *T* and often need suitable techniques for monitoring their hygro-thermal response. However, the main limit of the largely used sensor-based techniques is their ability to provide measurements only in specific locations of wood. Moreover, the development of accurate three-dimensional finite element (FEM) numerical models for moisture transport is important to improve the knowledge on the distribution of moisture content (*MC*) and temperature (*T*) inside wooden elements during their service life under various climates. The profound understanding on the hygro-thermal behaviour of wood can help engineers, architects, industries, administrations to develop better design, manufacturing and maintenance practices to improve the safety, serviceability and durability of wooden components.

The risks related to moisture content in wooden structures are due to the annual variations of relative humidity *RH* that increase the moisture penetration depth in wooden elements under variable climates (Svensson et al. 2011). For wood components sheltered from rain and sun and characterized by moisture states below the fibre saturation point (*FSP*), high daily variations of moisture contents in the presence of high levels of relative humidity above the 80% during drying, can cause very large moisture gradients in the vicinity of the external surfaces of the wood component, as well as moisture changes in internal locations. These moisture changes, along with the related constrained swelling and shrinkage in wood, are responsible of the so-called moisture induced stresses (*MIS*). (Fragiacomo et al. 2011, Fortino et al. 2013, Fortino et al 2019 a,b). The *MIS* can cause cracks in wooden components as, for example, glulam (Jönsson 2005, Angst 2012) and cross laminated timber (Gereke and Niemz 2007). The *MIS* perpendicular to grain may exceed the tensile and compressive strength also in the absence of external mechanical loads (Angst 2012). Peaks of moisture contents above 20-25% in wood components partially or fully exposed to outdoor climates are potentially dangerous for their durability and could increase in the presence of cracks propagating from the wood surface to the internal locations (Pousette et al 2017, Fortino et al 2019a). This risk is greater in the presence of rain events or water traps that can favourite moisture states above the *FSP*, characterized by free water transport in the lumens. These high levels of moisture accumulated in wood during long periods, in combination with favourable levels of temperature (*T*), can create conditions for the growth of fungi and decay (Fortino et al 2019a, Brischke and Mejer-Veltrup 2016) and seriously affect the durability of wood products (Mejer-Veltrup et al 2017).

Within the most used models for transient moisture transport, the single-phase (or single-Fickian) model simulates the diffusion of moisture content in wood considering the moisture content *MC*, or alternatively the moisture concentration, as the only variable of Fick's second law equation (Ormarsson 1999, Hanhijärvi 2005, Fortino et al. 2009, Fortino et al. 2011). However, as summarized in (Eitelberger et al. 2011a,b,c), single Fick's second law equation cannot accurately describe the transient moisture transport below the FSP because the water exists in the two phases of water vapour in the lumens and bound water in the cell walls.

In the last two decades, several multi-phase models for moisture transport in wood have been developed especially in the framework of heat and mass transfer to simulate the hygro-thermal response of wood under high temperature processes. Models including diffusion and thermo-diffusion (the so-called Soret effect) of moisture under non-isothermal conditions have been adopted by Eriksson (2006) and Trcala (2012). Multi-phase models for simulation of the moisture transfer under non-isothermal conditions for wood drying have been also presented in (Di Blasi 1998, Perré 1999, Younsi et al. 2007), including also the free water in lumens. In the above works there is an assumption of equilibrium between all phases of water in the wood domain at all times. Starting from 2003, there was an intensive research effort to develop the multi-phase moisture transport formulation for wood material below the FSP by defining the so-called multi-Fickian theory (Krabbenhoft 2003, Frandsen 2007). The multi-Fickian model considers the water vapour and bound water phases separately and the coupling between them is defined through the sorption rate between the two phases. Therefore, the multi-Fickian models below the FSP include two Fick's second law equations coupled by a sorption rate term. The use of another equation of energy conservation in the model formulation (Eitelberger et al. 2011b,c), allows to take into account the variable temperature. This is useful in the presence of continuously changing climates also for cases of large timber components of bridges (Fortino et al., 2013, 2019a,b). However, the multi-Fickian model is not yet developed to predict the moisture states above the FSP. For wooden components under ambient conditions, multi-phase models were proposed mainly in the field of building physics (Janssen et al. 2017). As summarized in the review presented in (Kang and Chung 2009), the building physics approach is to use a non-linear equation with only the moisture content as a variable and an effective diffusivity including contributions of all water phases, i.e. water vapour, bound water and free water. To model the effect of rain, simplified single-phase models with assigned high levels of moisture content on the boundaries were developed at Lund University in (Niklewski et al. 2016), also in conjunction with models for decay cause by fungi (Brischke and Mejer-Veltrup 2015).

In the present report, the material properties needed in different hygro-thermal numerical models are collected from the literature, as well as from recent projects in which some of the Click Design partners were involved. New sorption isotherms were measured within the Finnish national project DigiMoist1 (A Digital end user toolset for Moisture assessment in Wooden buildings. 1st part: Hygro-thermal database), funded by the Finnish Ministry of the Environment. The deliverable is shared for the scientific partners of Click Design. DigiMoist1 is actively collaborating with Click Design also thank to the common industrial partner Jartek Oy.

2. HYGRO-THERMAL MODELS

2.1 Background

2.2 Single-phase models for moisture states below the FSP

The Fick equation for moisture transport, defined on the wood sample can be written as

$$\frac{\partial c}{\partial t} = -\nabla \cdot \mathbf{J} \quad (1)$$

where c is the moisture concentration and $\mathbf{J}$ the moisture flux. In the case of single-phase models the $\mathbf{J}$ is defined as the moisture flux $\mathbf{J}_d$ below the fibre saturation point *FSP*. The first flux is related to an effective diffusion $\mathbf{D}_{eff}$ of moisture below the FSP that describes both the water vapour diffusion in pores and the bound water diffusion in wood cell walls, as usually done in the single-phase models for moisture transport:

$$\mathbf{J} = \mathbf{J}_{\boldsymbol{d}} = -\mathbf{D}_{\boldsymbol{eff}} \cdot \boldsymbol{\nabla} c \qquad (2)$$

The expressions of effective diffusion coefficients available in the literature, are collected in Table 1.

The moisture flux through the surface is given by the following equation:

$$\mathrm{J}_n = \rho_0 k_{em}(MC_{eq} + MC_{rain} - MC_{surf}) \qquad (3)$$

where

J_n = flux across the boundary [kg/m^{2}s]
ρ_0 = wood density in absolute dry conditions [kg/m^3]
k_{em} = surface emissivity [m/s]
MC_{eq} = moisture content of wood in equilibrium with the air humidity [-]
MC_{rain} = increase of liquid moisture content due to random rain or artificial spray water
MC_{surf} = moisture content solution on the wood surface [-]

Some literature expressions of MC_{eq} in function of the relative humidity, also called sorption isotherm, are collected in Table 2. The sorption isotherm represents the equilibrium between the relative humidity *RH* of the air and moisture content of wood *MC*. The *RH* represents the ratio between the partial vapour pressure p_v and the saturated vapour pressure p_{vs}. In Eq. (4) the semi-empirical Kirchhoff equation provide p_{vs} for the thermal ranges above the freezing point and Teten's fitting for ice defines p_{vs} in the subfreezing range (Frandsen 2007):

$$p_{vs} = \begin{cases} \exp\left(53.421 - \frac{6516.3}{T} - 4.125\ \ln(T)\right) & \text{for } T \geq 0°\text{C} \\ 100 \times 10^{\frac{9.5(T-273.15)}{T-7.65}+0.7858} & \text{for } T < 0°\text{C} \end{cases} \qquad (4)$$

The surface emission S (or surface emission coefficient) is related to the permeance k_v usually adopted in the coating industry, measured by the methods of wet or dry cup, and defined as

$$k_v = \frac{1}{\frac{1}{k_w} + \frac{1}{k_c}} \qquad (5)$$

where k_w is the permeance of the uncoated wood and k_c the permeance of the coating expressed in [kg/ m2 s Pa] units. To transform the permeance k_v in surface emission k_{em} [m/s], the saturated vapour pressure is used:

$$k_{em} = k_v p_{vs} c_{FSP} \qquad (6)$$

where c_{FSP} is the water concentration at the fibre saturation point. On the boundaries, Dirichlet conditions on the moisture content (fixed values of MC) can be also applied. The present model can include Dirichlet boundary conditions as, for example, fixed level of moisture contents on some external surface of the domain.

2.3 Simplified multi-phase models for moisture states below and above the FSP

In the case of simplified multi-phase models, the flux of equation (1) is defined as the sum of three components:

$$\mathbf{J} = \mathbf{J}_v + \mathbf{J}_b + \mathbf{J}_f \tag{7}$$

where $\mathbf{J}_v$, $\mathbf{J}_b$, $\mathbf{J}_f$ are the fluxes of water vapour in lumens, bound water in cell walls and free water in lumens, respectively. Equation 1 can be coupled with the energy conservation equation to take into account the variability of the temperature, as shown in Younsi (2006) and Fortino et al. (2013).

In the present review report, the multiphase model is further simplified considering a unique diffusion below the fire saturation point and the temperature in the whole body equal to the temperature of the air. Based on this assumptions, the moisture flux of equation (1) will be the sum of the effective diffusion flux and the free water flux:

$$\frac{\partial c}{\partial t} = -\boldsymbol{\nabla} \cdot (\mathbf{J}_d + \mathbf{J}_f) \tag{8}$$

Following Younsi et al. 2006, the transport of free water in pores above the FSP is governed by the generalized Darcy's law and the related flux is expressed as

$$\mathbf{J}_f = -\frac{\alpha\beta\rho_l(MC_{max}-MC_{FSP})^{\beta}}{\mu_l(MC-MC_{FSP})^{1+\beta}}\mathbf{K}_l \cdot \boldsymbol{\nabla} c = \mathbf{D}_f \cdot \boldsymbol{\nabla} c \tag{9}$$

with
α = parameter [-]
β = parameter [-]
ρ_l= liquid water density
μ_l = liquid viscosity
ε_d= dry wood void space
$\mathbf{K}_l$ = matrix of liquid permeability [m2]

Equation (8) can be also expressed in terms of a total diffusion $\mathbf{D}$ that refers to all phases of water and is defined here as the sum of the effective diffusion below the *FSP,*$\mathbf{D}_{eff}$ and the free water diffusion $\mathbf{D}_{free}$ above the *FSP*:

$$\frac{\partial c}{\partial t} = -\boldsymbol{\nabla} \cdot \mathbf{D} \cdot \boldsymbol{\nabla} c \tag{10}$$

$$\mathbf{D} = \mathbf{D}_{eff} + \mathbf{D}_{free} \tag{11}$$

Equation (9) is based on the assumption that the capillary pressure P_c depends only on the saturation S:

$$P_c = \alpha S^{-\beta} \tag{12}$$

$$S = \frac{MC-MC_{FSP}}{MC_{max}-MC_{FSP}} \tag{13}$$

where:

$MC_{max} = \varepsilon_d \frac{\rho_l}{\rho} + MC_{FSP}$ = maximum value of moisture content [-]

MC_{FSP} = value of moisture content at the fibre saturation point [-]

3. HYGRO-THERMAL PROPERTIES

The hygro-thermal properties reported in this section were collected from the literature in collaboration with partner Stora Enso.

3.1 Effective diffusion

A short review of the diffusion parameters available in the literature is shown in Table 1 and some measurements available in the literature are also presented in Figures 1-3. Figure 1 shows the range of the diffusion curves, in function of the moisture content, collected by Nilsson (1988) where also a review of the technologies for measurement of moisture diffusion is done.

Table 1 Effective diffusion coefficients for single-phase models

Transverse D [m2/s]	Longitudinal D [m2/s]	Reference
measurements	measurements	Koponen (1984)
based on literature (Figure …)		Nilsson (1988)
$1.5 \cdot 10^{-10}\, e^{2.28MC}$	$304 \cdot 10^{-10}\, e^{-17.7MC}$	Droin-Josserand et al. (1989)
$1.2 \cdot 10^{-10}\, e^{2.28MC}$		Toratti (1992)
$8.0 \cdot 10^{-11}\, e^{4.0MC}$		Hanhijärvi (1995)
calculations	calculations	Sjödin (2004), based on Siau's equations (1995)
$2.4 \cdot 10^{-10}\, e^{4.0MC}$		Fortino et al. (2009)
$3.0 \cdot 10^{-10}$, $9\% < MC < 16\%$		Angst (2012)

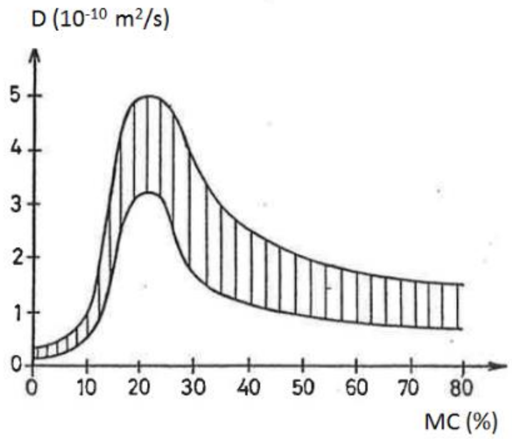

Figure 1 Range of diffusion curves in function of moisture content. Figure adapted from Nilsson (1988).

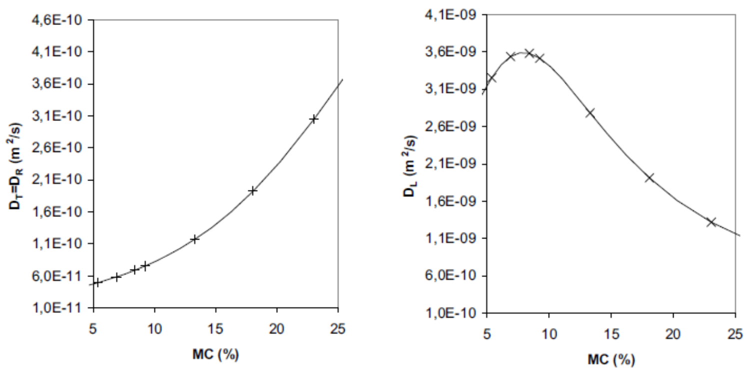

Figure 2 Diffusion curves in transversal (left) and longitudinal (right) directions of wood in function of moisture content (figure adapted from Sjödin 2004).

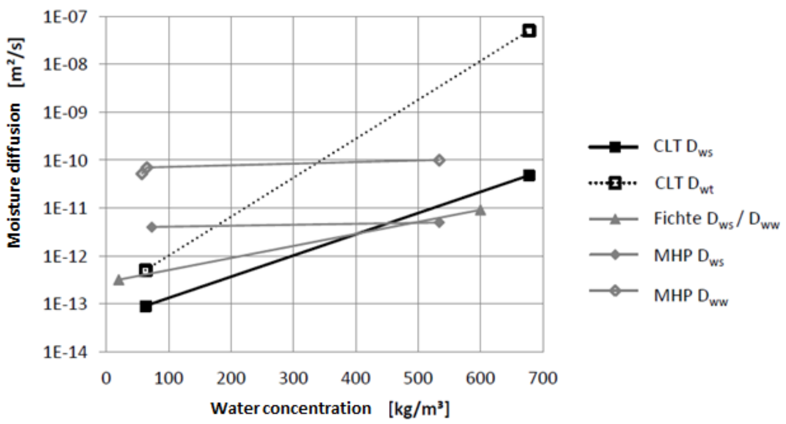

Figure 3 Measurements of moisture diffusion in function of water concentration for various wood species and wood products: CLT (cross laminated timber), Weichholz (softwood), Fichte (spruce), MHP (hardwood), KLH (massive wood). Figure adapted from (Hirsch 2013).

3.2 Sorption isotherms

Equations of sorption isotherms available in the literature are reported in in Figures 4-10 and Table 2. In the recent review work by Engelund Thybring et al (2017), the current techniques to measure the sorption isotherms below and above the fibre saturation point are discussed (see Figure 4). From the same paper, a review of the available sorption isotherms below and above the FSP (especially from the work of Maria Fredriksson group in Lund, see also Fredriksson and Johansson 2016) is shown in Figures 9-10.

New results from experiments on thermally modified wood, collecting sorption isotherms in adsorption and desorption, are reported in Section 5.

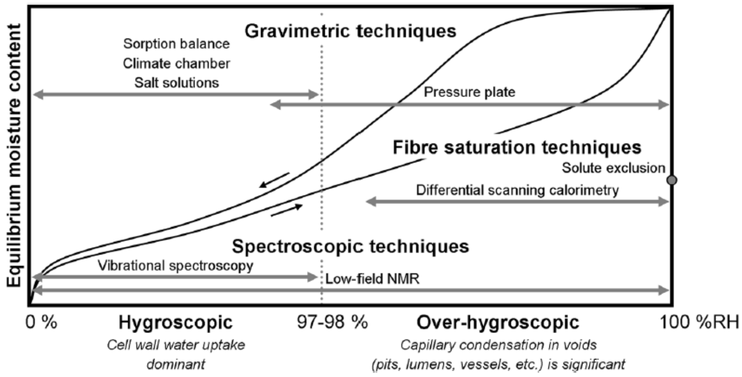

Figure 4 Schematic representation of the moisture uptake in wood during absorption from absolute dry state (lower black line) and desorption from fully water-saturated state (upper black line) in the entire relative humidity (RH) range from dry to water-saturated. Review of techniques (gravimetric, fibre saturation, and spectroscopic) along with the covered RH range. (Figure 1 from Engelund Thybring et al 2017).

Table 2 Sorption isotherms to be used in numerical models

<table>
<tr><th>sorption isotherm</th><th></th><th>Reference</th></tr>
<tr><td>$$MC_{eq} = 0.01\left(\frac{-T\,ln(1-RH)}{0.13\left(1-\frac{T}{647.1}\right)^{-6.46}}\right)^{\frac{1}{110\,T^{-0}}}$$</td><td></td><td>Avramidis (1989)</td></tr>
<tr><td>Hailwood – Harrobin model (reference in Frandsen 2007)
$$MC_{eq,\alpha} = \frac{RH}{f_{1\alpha} + f_{2\alpha}RH + f_{3\alpha}RH^2}$$
$\alpha = a, d$ (adsorption, desorption)</td><td>Temperature range: +20 … +25 Celsius (measurements, Ahlgren 1972)
<table><tr><th></th><th>$f_{1\alpha}$ [-]</th><th>$f_{2\alpha}$ [-]</th><th>$f_{3\alpha}$ [-]</th></tr><tr><td>a</td><td>1.804</td><td>13.63</td><td>-12.12</td></tr><tr><td>d</td><td>1.886</td><td>7.884</td><td>-6.526</td></tr></table></td><td>References in Frandsen (2007)</td></tr>
<tr><td>Andersson-McCharty model (reference in [])
$$MC_{eq,\alpha} = -\frac{\ln(\ln(1/h)/f_{1\alpha})}{f_{2\alpha}}$$
$$f_{i\alpha} = \sum_{j=0}^{n} b_{ij}^{\alpha}T^j,\ i \in \{1,2\}$$
$\alpha = a, d$ (adsorption, desorption)</td><td>Temperature range: 5… +25 Celsius (from review in Frandsen 2007, paper 6)
<table><tr><th>Species</th><th>α</th><th>n</th><th>b_{12}^{α} [K^{-2}]</th><th>b_{11}^{α} [K^{-1}]</th><th>b_{10}^{α}</th><th>b_{22}^{α} [K^{-2}]</th><th>b_{21}^{α} [K^{-1}]</th><th>b_{20}^{α}</th></tr><tr><td>?</td><td>?</td><td>1</td><td>0</td><td>−0.0143</td><td>7.73</td><td>0</td><td>0.0567</td><td>0.875</td></tr><tr><td>sitka spruce</td><td>d</td><td>2</td><td>-4.228×10^{-5}</td><td>0.0196</td><td>1.47</td><td>9.53×10^{-4}</td><td>−0.518</td><td>87.6</td></tr><tr><td>klinki pine</td><td>a</td><td>1</td><td>0</td><td>−0.0234</td><td>11.1</td><td>0</td><td>0.0657</td><td>0.0865</td></tr><tr><td>klinki pine</td><td>d</td><td>1</td><td>0</td><td>−0.0367</td><td>16.3</td><td>0</td><td>0.0535</td><td>2.13</td></tr></table>
Temperature range: -25 … +30 Celsius (fitted in Fortino et al. 2019a from measurements from Hedlin 1967)
<table><tr><th>α</th><th>n</th><th>b_{10}^{α} [-]</th><th>b_{11}^{α} [K^{-1}]</th><th>b_{20}^{α} [-]</th><th>b_{21}^{α} [K^{-1}]</th></tr><tr><td>a</td><td>1</td><td>7.719</td><td>-0.011</td><td>5.079</td><td>0.046</td></tr><tr><td>d</td><td>1</td><td>9.739</td><td>-0.017</td><td>-13.419</td><td>0.100</td></tr></table></td><td>References in Frandsen (2007) and Fortino et al. (2019,a)</td></tr>
</table>

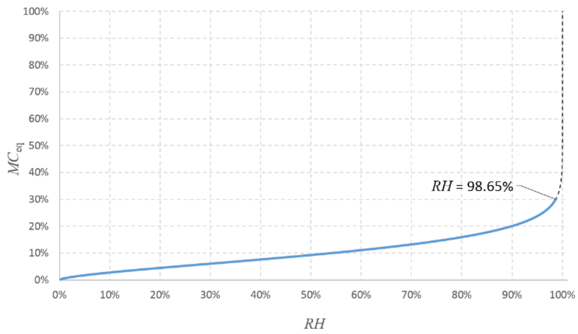

Figure 5 Sorption isotherm from Avramidis (1989). In black dashed line the part of the curve affecting the moisture state above the fibre saturation point (MC=30%) in the simplified multi-phase numerical model.

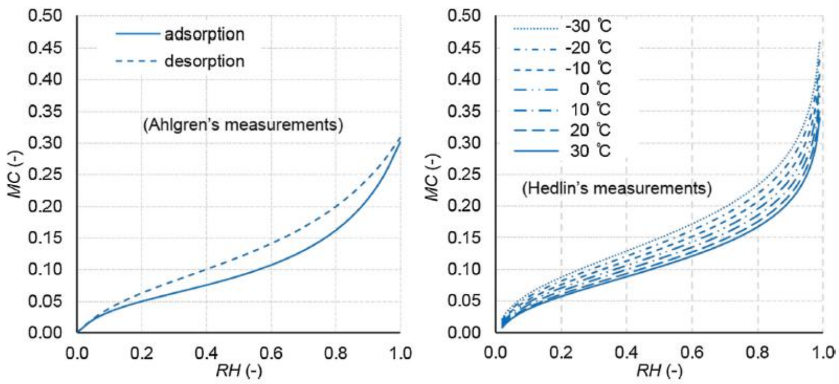

Figure 6 Left: Hailwood – Harrobin adsorption and desorption curves fitted on Ahlgren´s measurements at *T*=23̊C (reference in Frandsen 2007). Right: Anderson-McCarty average sorption curves at different temperatures extrapolated from Hedlin´s measurements (interpolated in Fortino et al. 2019a9.

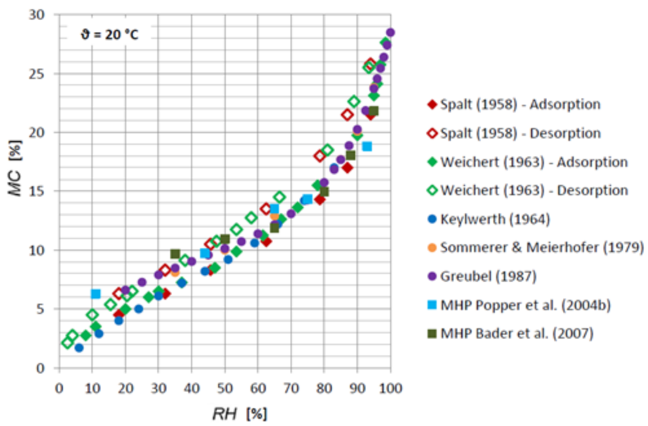

Figure 7 Measurements of adsorption and desorption isotherms. Figure adapted from (Hirsch 2013).

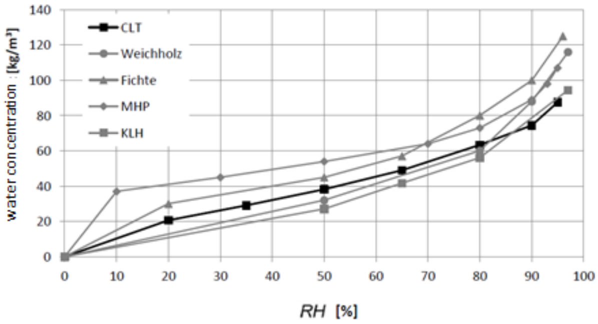

Figure 8 Measurements of adsorption and desorption isotherms, relative humidity in function of water concentration for various wood species and wood products: CLT (cross laminated timber), Weichholz (softwood), Fichte (spruce), MHP (hardwood), KLH (massive wood). Figure adapted from (Hirsch 2013).

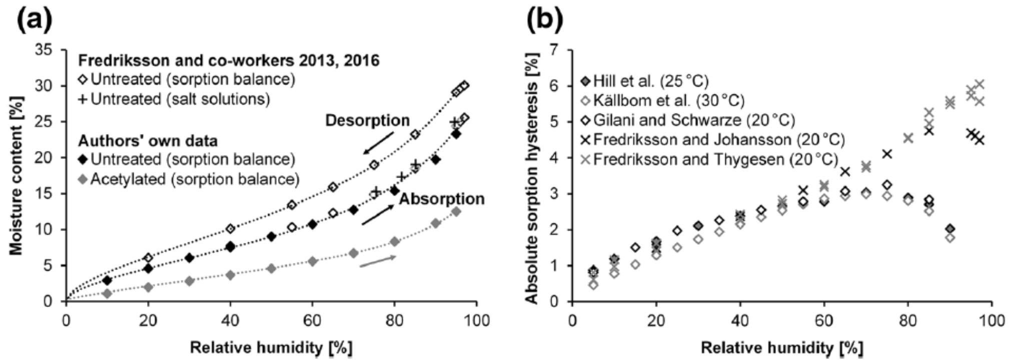

Figure 9 (a) Sorption isotherms for desorption from water-saturated state and absorption from dry state for untreated and acetylated. Norway spruce in the range of 0–97% relative humidity (RH). (b) absolute sorption hysteresis of untreated wood from moisture content data acquired with automated sorption balances. Based on data for Norway spruce. (Figure 2 and related references from Engelund Thybring et al. 2017).

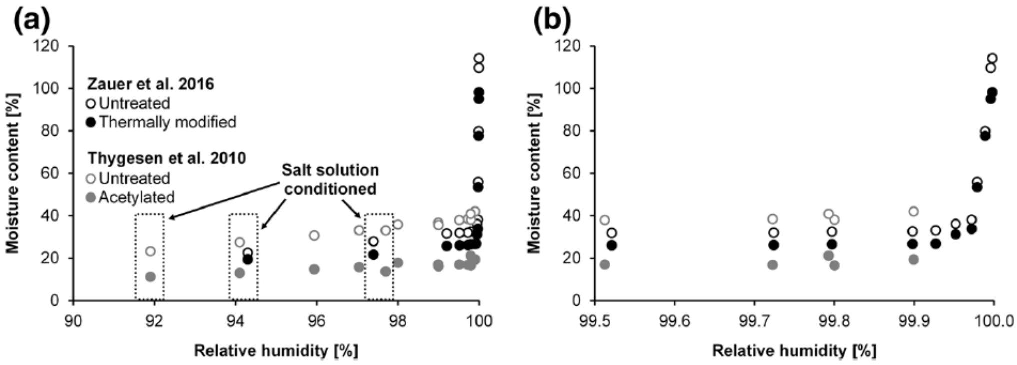

Figure 10 (a) Desorption isotherms in the over-hygroscopic range determined after conditioning with the pressure plate technique and saturated salt solutions for untreated and modified Norway spruce. (b) Zoom of (a) in the 99.5–100.0% RH range. (Figure 3 from Engelund Thybring et al. 2017).

4. PROPERTIES FOR THE COUPLED DIFFUSION-PERMEABILITY MODEL

The simplified multi-phase model including effective diffusion below the fibre saturation point FSP and the free water diffusion (including the liquid permeability) above FPS, described in the previous section, needs suitable material properties. For the diffusion below the FSP, an average of the diffusion curves collected by Nilsson (1988), in transverse direction, and by Koponen (1984), in longitudinal direction, is connected to the free diffusion presented in Younsi et al (2006). The value of the liquid permeability in transversal direction is taken from (Pang 2007) and the one in the longitudinal direction is assumed to be 1000 times larger, following Perré and Turner (2002), see Table 3 and Figure 11.

Table 3 Parameters for the simplified multi-phase model (Fortino, Hradil, Dohnal, Nie, Musci, Metelli, 2020, unpublished)

Parameter/physic quantity			units
parameter of saturation	α	1000	(-)
parameter of saturation	β	0.61	(-)
dry wood void space	ε_d	71%	%
Liquid water viscosity	μ_l	1.002	kg/ m s
liquid water density	ρ_l	1000	kg/m3
(MC at FSP)	MC_{FSP}	28	%
Liquid permeability in transversal direction	K_{lt}	4E-15	m2
Liquid permeability in longitudinal direction	K_{lL}	4E-12	m2

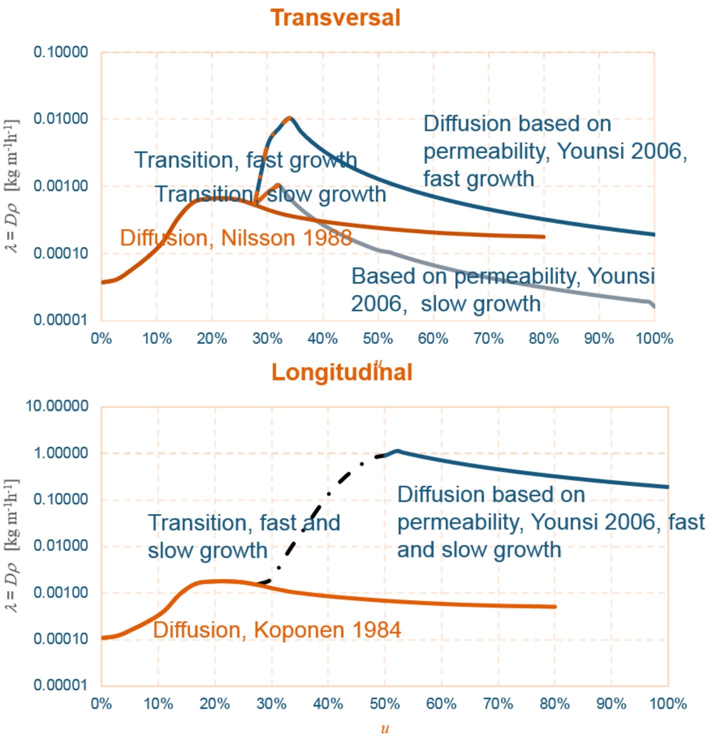

Figure 11 Coupled effective diffusion-permeability curves for simplified multi-phase models. Density ρ=450 kg/m3 (Fortino S. and Nie Y., 2020, unpublished).

4.1 Capillary pressure, saturation and permeability

For moisture states above the FSP, a good review about empirical equations for capillary pressure-saturation in wood is done in (Khang and Chung 2009) and reported in Table 4. Capillary pressures vs saturation and liquid permeability vs wood density were reported by Perré and Turner (2001) see Figures 10 and 11.

Table 4 Empirical equations for capillary pressure-saturation in wood. Table taken from (Khang and Chung 2009 and the related references 4,13,15,15)

Equation	Constants	Species	Reference
$P_c(S) = a_1 S^{-a_2}$	$a_1 = 8.4 \times 10^4$, $a_2 = 0.63$	Southern pine	4
$P_c(S,T) = 101325[a_1 S \exp(-a_2 S) + a_3(1-S)S^{-a_4}](1-2.79 \cdot 10^{-3}(T-273))$	Heartwood $a_1 = 12.12$, $a_2 = 5.939$, $a_3 = 0.046$, $a_4 = 3.7$ Sapwood $a_1 = 1.937$, $a_2 = 3.785$, $a_3 = 0.093$, $a_4 = 1.4$	Pine	13
$P_c(S,T,\rho) = \sigma(T)\left[\frac{a_1}{S+a_2} - \frac{a_3 + a_4\rho_0}{a_5 - S} + a_6\rho_0(1-S) + a_7 + a_8\rho_0 - \frac{a_9}{1+a_{10}}\right]$	$a_1 = 3150$, $a_2 = 1.0 \times 10^{-4}$, $a_3 = 1047$, $a_4 = 3.368$, $a_5 = 1.02$, $a_6 = 149.8$, $a_7 = 52\ 350$, $a_8 = 168.4$, $a_9 = 3150$, $a_{10} = 1.0 \times 10^{-4}$	Softwood	14
$P_c(S,T) = \sigma(T)\sqrt{\frac{\phi}{K_w}}J(S)$, $J(S) = \frac{a_1}{S-a_2} + \frac{a_3}{S+a_4} - a_5 S + a_6$	$a_1 = 9.547 \times 10^{-3}$, $a_2 = 1.028$, $a_3 = 2.0023 \times 10^{-2}$, $a_4 = 0.0$, $a_5 = 1.2 \times 10^{-5}$, $a_6 = 4.415 \times 10^{-3}$	Bed of glass spheres	15

$\sigma(T) = (77.5 - 0.185(T - 273.15)) \times 10^{-3}$

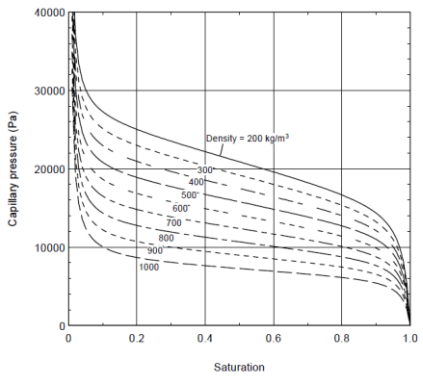

Figure 12 Capillary pressure vs saturation for different wood densities (figure from Perré and Turner, 2001).

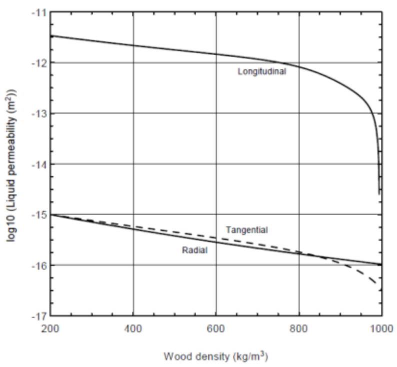

Figure 13 Liquid permeability vs wood density in transverse and longitudinal directions of wood (figure from Perré and Turner, 2001).

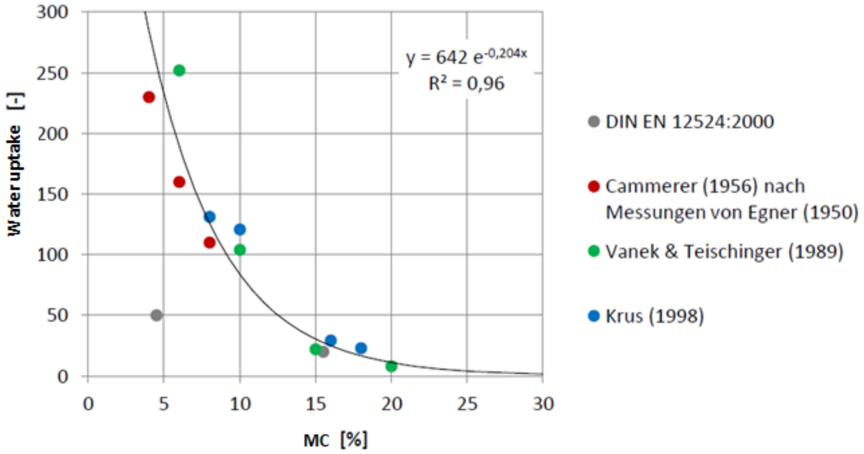

Figure 14 Measurements of water uptake in function of moisture content. Adapted from (Maren Hirsch 2013, MSc Thesis).

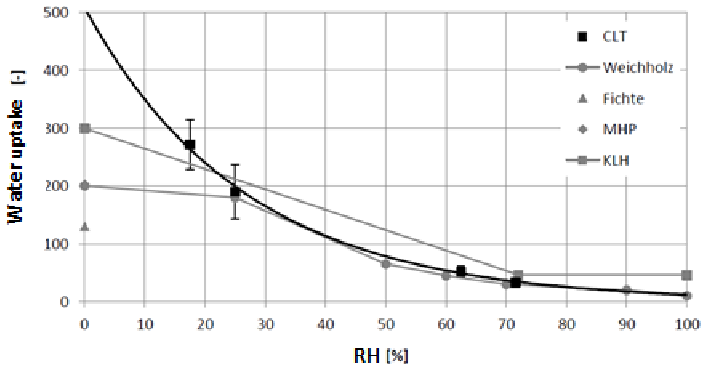

Figure 15 Measurements of water uptake in function of the relative humidity for various wood species and wood products: CLT (cross laminated timber), Weichholz (softwood), Fichte (spruce), MHP (hardwood), KLH (massive wood). Adapted from (Maren Hirsch 2013, MSc Thesis).

4.2 Moisture resistance for coated wood

In Table 5 some measured values of moisture resistance (or water vapour resistance), i.e. the inverse of the permeance, are listed for various paints and wall coverings. Lower values indicate an increased potential for utilization of the moisture buffering capacity of the underlayer.

In a document by Koponen (2002), it is pointed out that the moisture resistance of paints depends on the ambient relative humidity as well as on the moisture content of the substrate. The values of permeance collected by Koponen are listed in Appendix A. The permeances measured with the method of the wet cup are usually 3-5 times higher than those measured by the dry cup method. The amount of pigments affects the permeability which increase with the increasing pigment amount. However, the addition of pigments deteriorates other paint properties, such as the abrasion resistance and the washability.

Table 5 Moisture resistance of paints with thickness 0.05 mm (Berge 2009)

Surface treatment Vapour diffusion resistance	Vapour diffusion resistance ($10^9 m^2 sPa/kg$)
Cement paints	0.4
Lime paints	0.2
Silicate paints	0.2–1.0
Acrylate paints/varnishes	0.7–2.7
Alkyd oil paints	2.5–5
Alkyd oil varnishes	19–39
Epoxy paints	40–50
Epoxy varnishes	39–72
Polyurethane varnishes	50
Collagen glue paints	0.2–0.3
Linseed oil, not pigmented	0.9–1.0
Linseed oil paints	1.0–3.5

5. SORPTION ISOTHERMS FOR THERMALLY TREATED WOOD - NEW MEASUREMENTS

The work reported in this section was performed by partner Jartek Invest at Aalto University.

Commercially produced (Southern Finland) Thermowood board of Scots pine (*Pinus sylvestris L.*) was used and cut to 10 x 10 x 10 mm dimensions. The material was free of knots and visible defects. Prior to testing, samples were dried at 20°C and RH 50% for one month. The size of the samples was 3 × 3 mm (radial × tangential) dimensions, and longitudinal dimension was changed to meet the required mass of 15 mg. Care was taken that the samples contained both, early- and latewood at a constant ratio. Therefore, this factor was not considered during data analysis.

The experiments were carried out in a DVS (DVS Intrinsic, Surface Measurement Systems Ltd., London, UK), coupled with liquid deionized water at various temperatures from 20 °C to 40 °C and a gas flow of 200 cm^3 min^{-1}. In the initial drying step, the samples were first dried at 0 % RH until the mass change rate (dm dt^{-1}) remained at 0.002 % for 10 minutes. This was followed by a rewetting step, where the samples were conditioned at 95 % RH (water vapour) for 24 hours and finally dried for 24 hours in 0 % RH. After that the sorption measurements were carried out with steps of 5 % RH from 0 % RH to 95 % RH and revised. 0.002 % mass change rate (dm dt^{-1}) for 10 minutes was used in step change criteria.

The results are reported in Table 6.

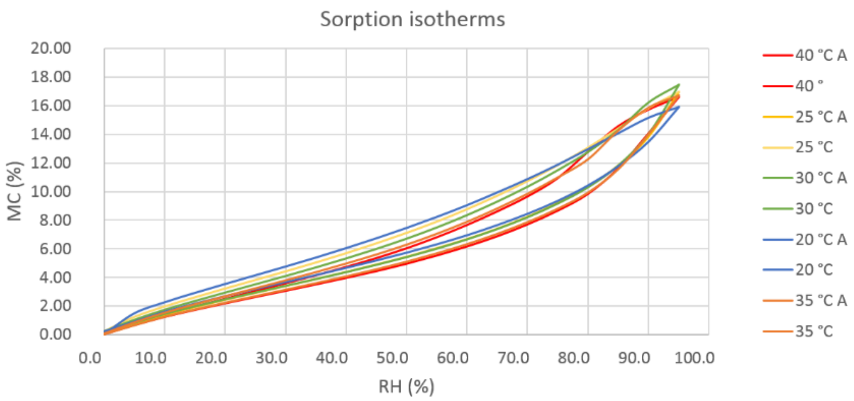

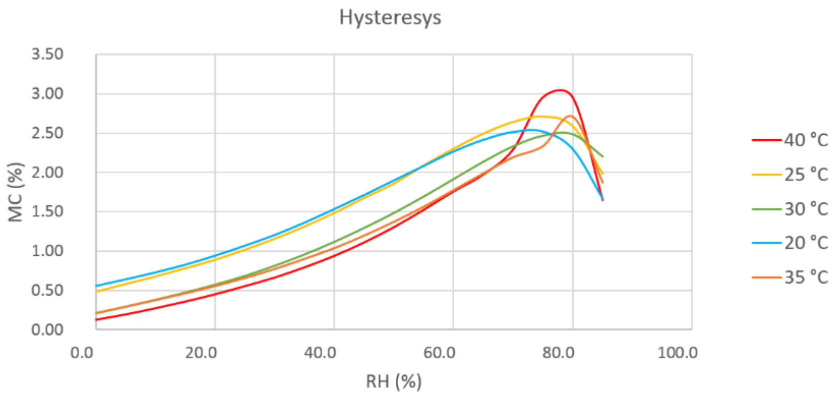

Figure 16 Thermally treated spruce wood (TW). Measurements of adsorption and desorption isotherms (top) and hysteresis (bottom).

Table 6 Thermally treated spruce. Measured moisture contents in adsorption, desorption and the related hysteresis at different relative humidities.

	T = 20 °C			T = 25 °C			T = 30 °C		
	Change in mass (%)			Change in mass (%)			Change in mass (%)		
RH (%)	Ads	Des	Hys	Ads	Des	Hys	Ads	Des	Hys
0.0	0.25	0.02		0.05	0.24		0.24	0.25	
5.0	0.93	1.48	0.56	0.77	1.25	0.48	0.84	1.05	0.21
10.0	1.62	2.26	0.64	1.41	1.98	0.58	1.46	1.75	0.29
15.0	2.19	2.91	0.73	1.95	2.62	0.67	1.99	2.37	0.38
20.0	2.71	3.53	0.83	2.46	3.23	0.78	2.48	2.96	0.47
25.0	3.20	4.14	0.94	2.95	3.83	0.88	2.96	3.53	0.57
30.0	3.68	4.75	1.07	3.42	4.43	1.01	3.42	4.11	0.68
35.0	4.17	5.38	1.20	3.90	5.05	1.15	3.89	4.71	0.81
40.0	4.67	6.04	1.36	4.40	5.70	1.31	4.38	5.34	0.96
45.0	5.19	6.73	1.54	4.91	6.39	1.48	4.89	6.00	1.12
50.0	5.74	7.45	1.71	5.45	7.13	1.67	5.43	6.72	1.29
55.0	6.32	8.22	1.90	6.06	7.91	1.85	6.02	7.50	1.48
60.0	6.95	9.04	2.09	6.69	8.78	2.08	6.67	8.36	1.69

65.0	7.66	9.93	2.27	7.42	9.72	2.30	7.39	9.31	1.91
70.0	8.45	10.87	2.42	8.25	10.74	2.49	8.21	10.35	2.13
75.0	9.35	11.87	2.52	9.22	11.86	2.64	9.17	11.50	2.33
80.0	10.43	12.95	2.52	10.37	13.08	2.71	10.31	12.77	2.46
85.0	11.77	14.06	2.30	11.84	14.43	2.58	11.83	14.31	2.48
90.0	13.48	15.15	1.67	13.85	15.83	1.98	14.03	16.23	2.20
95.0	15.90	15.90		16.97	16.97		17.46	17.46	

	T = 35 °C			T = 40 °C		
	Change in mass (%)			Change in mass (%)		
RH (%)	**Ads**	**Des**	**Hys**	**Ads**	**Des**	**Hys**
0.0	0.02	0.07		0.00	0.05	
5.0	0.65	0.85	0.20	0.65	0.78	0.13
10.0	1.24	1.53	0.29	1.21	1.41	0.20
15.0	1.75	2.13	0.37	1.70	1.98	0.28
20.0	2.23	2.69	0.46	2.17	2.53	0.36
25.0	2.69	3.24	0.55	2.61	3.06	0.45
30.0	3.14	3.80	0.65	3.05	3.61	0.56
35.0	3.60	4.37	0.77	3.49	4.16	0.67
40.0	4.07	4.97	0.90	3.95	4.74	0.80
45.0	4.57	5.61	1.03	4.42	5.36	0.94
50.0	5.10	6.29	1.19	4.94	6.05	1.11
55.0	5.69	7.06	1.37	5.51	6.82	1.31
60.0	6.33	7.90	1.56	6.15	7.68	1.53
65.0	7.06	8.83	1.77	6.86	8.62	1.76
70.0	7.87	9.86	1.99	7.69	9.67	1.98
75.0	8.81	11.01	2.19	8.66	10.95	2.30
80.0	9.95	12.28	2.33	9.83	12.79	2.96
85.0	11.58	14.29	2.71	11.63	14.58	2.95
90.0	14.02	15.89	1.87	14.08	15.73	1.65
95.0	16.73	16.73		16.61	16.61	

6. DIGIMOIST TOOLSET

The structure and modules of the *DigiMoist toolset* built within DigiMoist1 project are represented in Figure 17. The tasks in the blue boxes have been developed in DigiMoist1 project. The tasks in green boxes receive inputs and outputs from the on-going ForestValue ClickDesign project. The task in yellow boxes will be eventually developed in a future project.

The Finnish locations selected for the pre-calculations carried out in DigiMoist1 project are shown in Figure 1. The climates in the chosen cities are to be considered as representative climates for the different impacts of moisture in wood components of buildings in South, Centre and North Finland. They are also representative for the same type of climates in Europe and out of Europe.

In the following sections, the results of the numerical pre-calculations in terms of moisture gradients and moisture contents with the related risks of cracking and decay will be represented in the map of Finland.

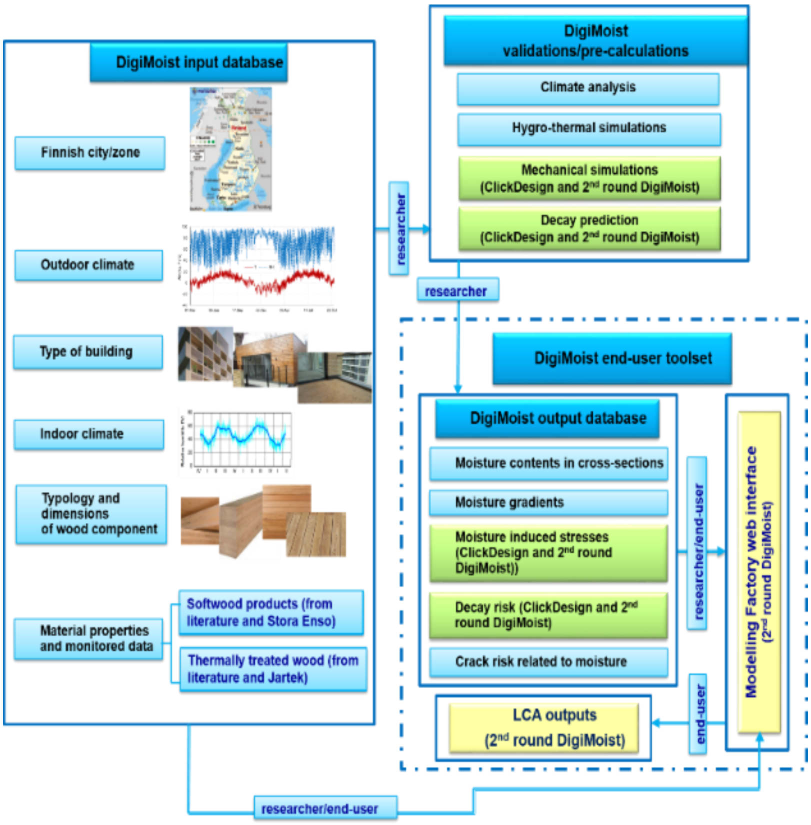

Figure 17 Structure of the general *DigiMoist toolset*. Selection of Finnish locations for hygro-thermal calculations.

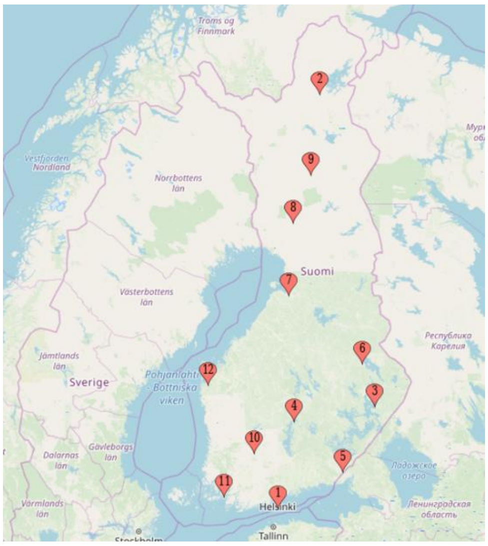

Figure 18 The 12 selected cities in Finland (1: Helsinki, 2: Inari, 3: Joensuu, 4: Jyväskylä, 5: Lappeenranta, 6: Nurmes, 7: Oulu, 8: Rovaniemi, 9: Sodankylä, 10: Tampere, 11: Turku, 12: Vaasa).

7. Climate module

The collected module components were the following:

- Outdoor climate database referring to European website https://www.ecmwf.int/ for the wooden elements exposed to outdoor climates in order to extract the data on relative humidity and temperature of the air, millimetres of rain for the selected Finnish cities. This is already available among the tools of HYGRO project at VTT (see for example the Helsinki weather in Figure 30).
- Definition of typical reference weathers based on Meteonorm code were provided to VTT by Click Design partner Lund University (https://aiguasol.coop/energy-software/meteonorm-7-2-global-weather-data/).

8. Pre-calculation module for Glulam and CLT cross sections

Finite element (FEM) pre-calculations were carried out for Glulam and CLT cross sections by using the commercial code Abaqus where the moisture transport models were implemented in user subroutines.

The pre-calculations were carried out for each city weather for the following different cross section sizes of Glulam and CLT (see the component typologies in Figure 19):

Glulam Middle lamella:

- 60 mm, 120 mm, 200 mm

Glulam Top lamella:

- 60 mm, 120 mm, 200 mm

CLT 3S (3 layers):

- 60 mm, 120 mm

CLT 3S (5 layers):

- 100 mm, 200 mm

Figure 19 Left: Glulam (analyzed top and middle lamellas have sizes of 60 mm, 120 mm and 200 mm). Right: CLT (analyzed 3S and 5S have sizes of 100 mm and 200 mm).

Referring to the water vapour resistance in Figure 20, the following cases of external surfaces were calculated for the various typologies of cross section:

- untreated wood
- weak coating, surface resistance = 1.E+07 m^2sPa/kg
- standard coating, surface resistance = 1.E+09 m^2sPa/kg
- strong coating, surface resistance = 1.E+10 m^2sPa/kg

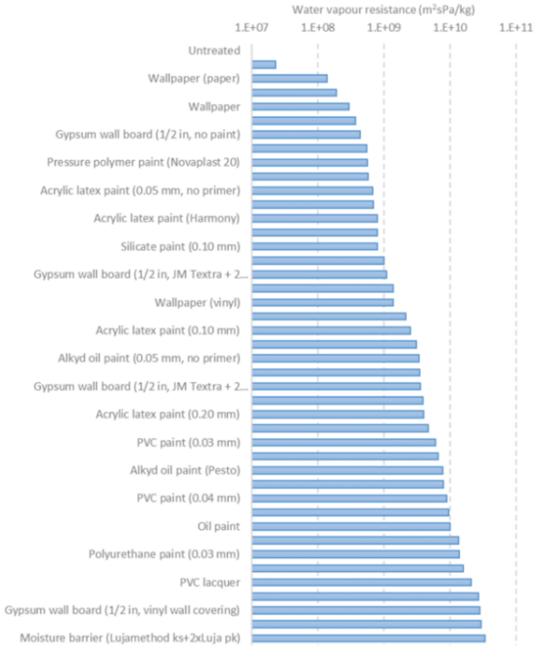

Figure 20 Water vapour resistance (surface resistance) for the surfaces of the analyzed cross sections.

The hygro-thermal material properties used in the analyses are the ones assessed for Norway Spruce. The effect of rain is not considered in the models and therefore the results are related to wood components under outdoor conditions but sheltered from rain. The initial moisture content is 16%. A pre-calculation time of 2 years was considered and the results refer to a successive analysis time of 1 year. The finite element mesh size used in the calculations if 5 mm.

8.1 Output Module for Glulam and CLT cases

Detailed examples of outputs are presented in Tables 7 and 8 for the cases of moisture content at 10 mm depth and the moisture gradients at 10 mm depth in Glulam cross sections. Plots of moisture contents, moisture envelops and moisture gradients are shown in Figures 21-23. The large amount of outputs and plots for the various cases studied in the project are available for the funders and partners in a shared workspace. All these data are planned to be used for the implementation of the *DigiMoist toolset* in the VTT Web Factory platform in future projects.

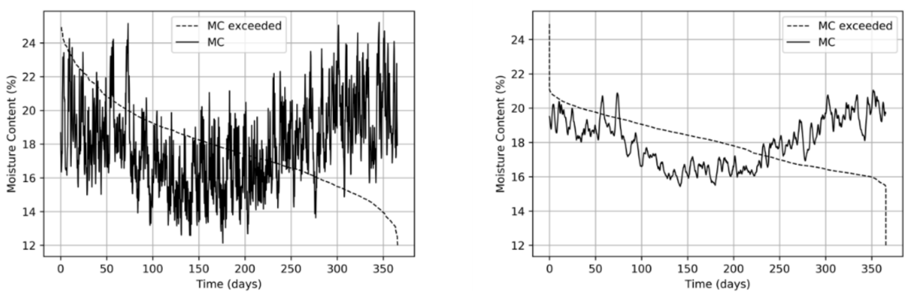

Figure 21 Helsinki weather. Glulam, middle lamella, 60 mm. Untreated surface. Moisture content (MC) and number of days in which each MC is exceded. Left: on the surface. Right: at 10 mm from the surface.

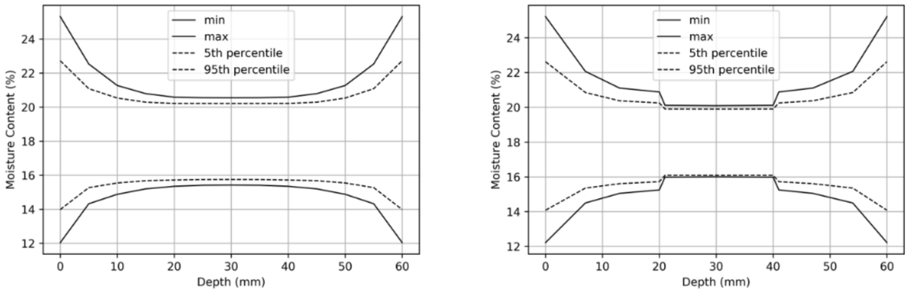

Figure 22 Helsinki weather. Moisture envelops. Left: Glulam, middle lamella, 60 mm. Right: CLT 3S (3 layers, 60 mm. Untreated surfaces.

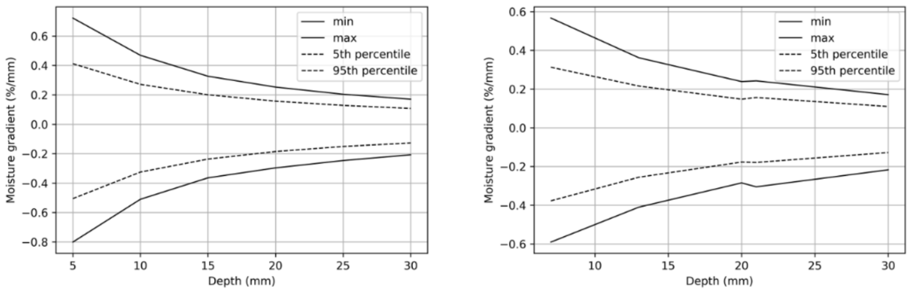

Figure 23 Helsinki weather. Moisture gradients. Left: Glulam, middle lamella, 60 mm. Right: CLT 3S (3 layers, 60 mm. Untreated surfaces.

Table 7 Helsinki weather, Glulam. Moisture contents at 10 mm depth.

		Untreated		Weak coating		Standard coating		Strong coating	
		min	max	min	max	min	max	min	max
Midle lamella	60 mm	14.9%	21.3%	14.9%	21.2%	15.2%	20.2%	16.7%	18.7%
	120 mm	15.4%	21.1%	15.4%	21.0%	15.7%	19.7%	17.0%	18.2%
	200 mm	15.5%	20.9%	15.5%	20.9%	15.8%	19.6%	16.8%	18.0%
Top lamella	60 mm	14.6%	21.5%	14.6%	21.5%	14.8%	20.5%	16.2%	19.0%
	120 mm	14.8%	21.5%	14.8%	21.4%	15.0%	20.4%	16.5%	18.8%
	200 mm	14.8%	21.5%	14.8%	21.4%	15.1%	20.3%	16.6%	18.7%

Table 8 Helsinki weather, Glulam. Moisture gradients at 10 mm depth.

		Untreated		Weak coating		Standard coating		Strong coating	
		min	max	min	max	min	max	min	max
Midle lamella	60 mm	-3.64 m-1	3.27 m-1	-3.58 m-1	3.23 m-1	-1.66 m-1	1.60 m-1	-0.39 m-1	0.30 m-1
	120 mm	-3.83 m-1	3.11 m-1	-3.76 m-1	3.08 m-1	-1.78 m-1	1.67 m-1	-0.40 m-1	0.32 m-1
	200 mm	-3.80 m-1	3.05 m-1	-3.75 m-1	3.03 m-1	-1.77 m-1	1.61 m-1	-0.41 m-1	0.31 m-1
Top lamella	60 mm	-3.69 m-1	3.41 m-1	-3.63 m-1	3.37 m-1	-1.65 m-1	1.57 m-1	-0.37 m-1	0.30 m-1
	120 mm	-3.72 m-1	3.30 m-1	-3.66 m-1	3.25 m-1	-1.64 m-1	1.59 m-1	-0.39 m-1	0.32 m-1
	200 mm	-3.73 m-1	3.28 m-1	-3.67 m-1	3.24 m-1	-1.64 m-1	1.59 m-1	-0.39 m-1	0.32 m-1

For the easier understanding of the large amount of outputs, the variation of maximum moisture gradients and moisture contents for the various cases are summarized on the map of Finland by contours. The high moisture gradients can indicate a risk of cracking related to the development of moisture induced stresses, while the high levels of moisture content above 25% can indicate a risk of decay. An example for the Glulam case, middle lamella, 60 mm, is shown in Figure 24 and an example for the 3 layer uncoated CLT case is presented in Figure 25. All the other cases for the middle lamellas are available in Appendix A. The top lamella cases are available in a shared workspace.

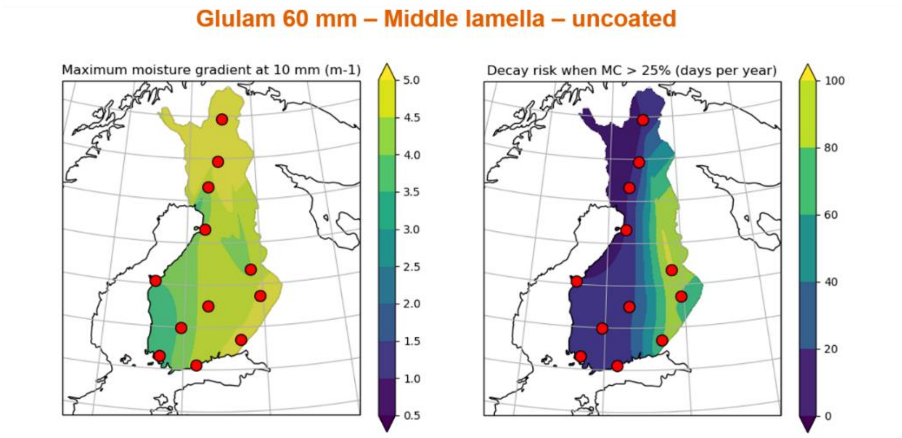

Figure 24 Left: Distribution of maximum moisture gradients in Finland for Glulam, middle lamella, 60 mm, uncoated. Right: Distribution of moisture content over 25% (days per year) for the same cross section.

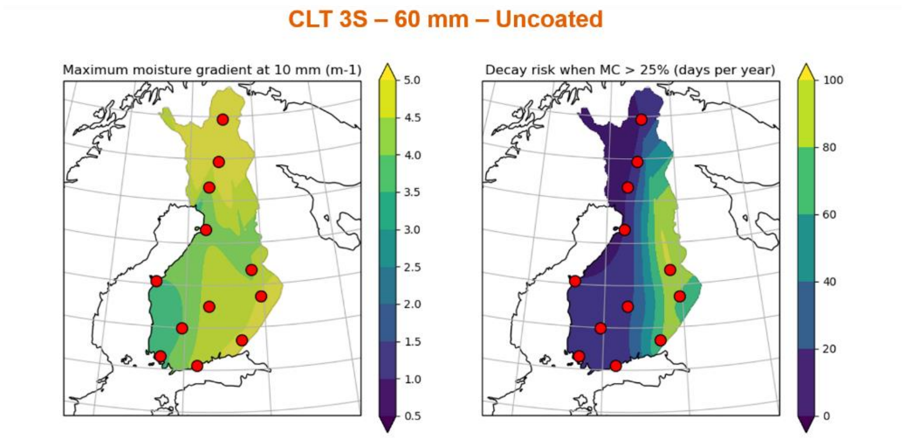

Figure 25 Left: Distribution of maximum moisture gradients in Finland for CLT 3S (3 layers), 60 mm, uncoated. Right: Distribution of moisture content over 25% (days per year) for the same cross section.

9. FIRST RESULTS FOR MOISTURE AND DECAY IN SOFTWOOD AND THERMOWOOD DECKING COMPONENTS

Based on the measurements of sorption isotherms performed by partner Jartek (Section 5), a model for moisture transport in Thermowood was created by using the diffusion-permeability approach presented in Section 4.

The difference between fitted sorption curves for untreated and TW softwood below and above the FSP is shown in Figure 26 at a temperature of 20 ^{0}C. The sorption curves for TW are defined by using the same equation adopted for untreated wood (Avramidis 1989, see Table 2), where coefficient 0.23 is used in place of 0.13.

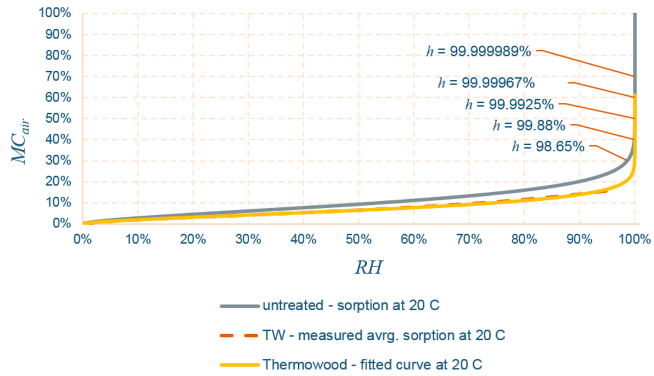

Figure 26 Sorption isotherms at T=20 °C used for untreated softwood (Norway spruce) and spruce Thermowood (TW).

In addition, the density of TW is 10% lower than the one of the untreated wood. The values used in the analysis are ρ_w=450 kg/m^3 for the untreated spruce and ρ_{TW}=405 kg/m^3 for the spruce Thermowood. The used diffusion-permeability properties are an average between the properties for fast grown and slow grown spruce wood shown in Figure 11.

Thank to the collaboration with project Click Design, it was also possible to simulate the decay due to brown rots in softwood and spruce Thermowood. The modelling uses te concept of dose, introduced in (Brischke and Meyer-Veltrup 2016). The dose, which is a function of the moisture content and temperature in wood (Figure 27a), can be also defined as a function of the decay rate used in the Eurocodes to explain the decay of wood due to moisture (Figure 27b).

$$D_u(u) = \begin{cases} 0 & \text{if} \quad u < 25\ \% \\ e \cdot u^5 - f \cdot u^4 + g \cdot u^3 - h \cdot u^2 + i \cdot u - j & \text{if} \quad u \geq 25\ \% \end{cases}$$

$$D_T(T) = \begin{cases} 0 & \text{if} \quad T_{\min} < 0\ °\text{C} \quad \text{or} \quad \text{if } T_{\max} > 40\ °\text{C} \\ k \cdot T^4 + l \cdot T^3 - m \cdot T^2 + q \cdot T & \text{if} \quad T_{\min} < 0\ °\text{C} \quad \text{or} \quad \text{if } T_{\max} < 40\ °\text{C} \end{cases}$$

$$D = (a \cdot D_T[T] + D_u[u]) \cdot (a+1)^{-1} \quad \text{if} \quad D_u > 0 \quad \text{and} \quad D_T > 0$$

Figure 27a Definition of dose. Top: equations of dose D taken. In the equations, *u* represents the moisture content. Figure adapted from (Metsä-Kortelainen and Viitanen 2015).

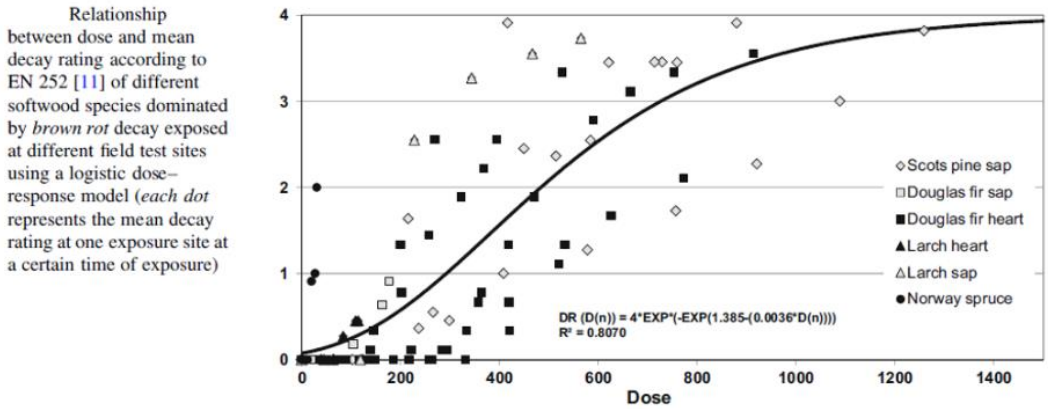

Figure 27b Definition of dose. Figure and equations taken from (Brischke and Meyer-Veltrup 2016).

9.1 Modelling of two-layered decking board cross sections

The modelling was aimed to simulate the hygro-thermal and decay behaviour of two-layered decking board cross sections. As reference data, some measurements carried out at VTT in earlier projects were used (Metsä-Kortelainen and Viitanen, 2015), see Figure 28. The tested system was a modified double layer test composed by base boards on the ground and a two-layered decking above the ground. The wood species tested, for both sapwood and hearthwood cases, are shown in Table 9. A scheme explaining the moisture effects in the two-layered decking is shown in Figure 29, left. In the present work, only the cross section of a representative cross section of the top board, located in the middle of the two-layered decking system, was modelled (Figure 29, right).

In the original experiments, the boards were placed in Otaniemi (Espoo), in the VTT area under outdoor climate from 2004 and 2010. The climate is almost the same as the available Helsinki weather (Figure 30). After the 6 years test, the final moisture content was measured and the decay level was estimated (see Figures 31 and 32).

The used diffusion properties available in DigiMoist1 for untreated spruce and spruce Thermowood, are in the range of slow and fast growth properties shown in Figure 11. Untreated spruce and Thermowood samples of cross section size 28 × 150 (Table 9) were analysed under the 6 years Helsinki weather (Figure 31). The results in terms of moisture content versus time are reported in Figures 33 and 36 and the results in terms of moisture distribution and dose distribution are presented in Figures 34 and 35 after 1 year analysis and in Figures 36 and 37 after 6 years analysis.

The decay ratings, functions of the annual doses according to Figure 27b, are reported in Table 10. In (Metsä-Kortelainen and Viitanen 2015) a different evaluation of decay was used which referred to decay rates.

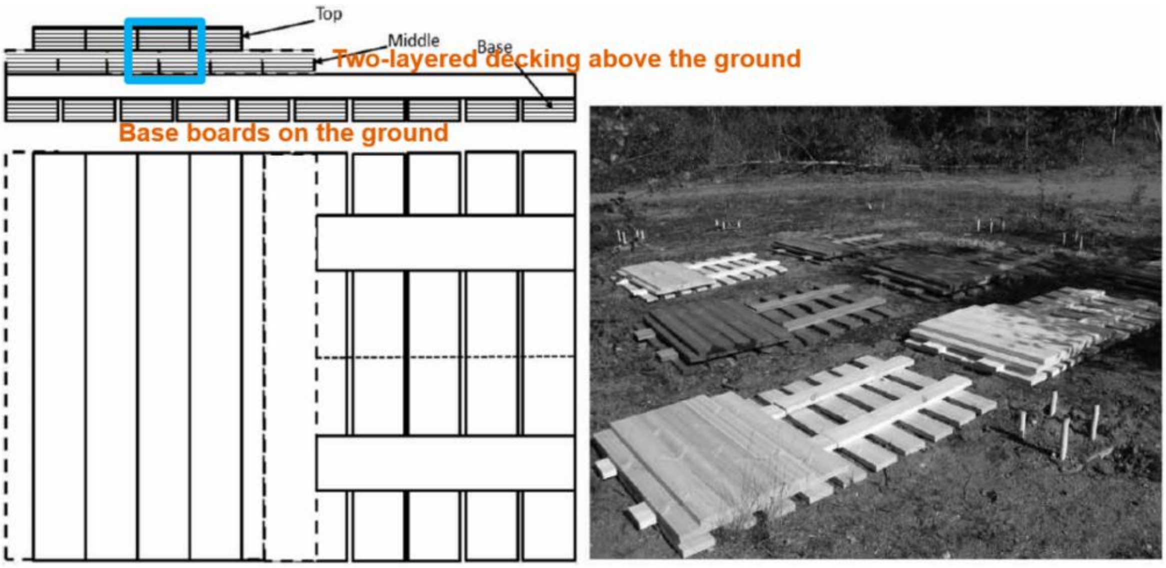

Schematic description of modified double layer test elements (left) and double layer elements in the field (right).

Figure 28. Description of the double layer system. Figures adapted from Metsä-Kortelainen and Viitanen (2015).

Table 9. Tested wood materials. Table adapted from (Metsä-Kortelainen and Viitanen 2015).

Wood material	Dimension (mm)	Replicate boards	MC (%)
Scots pine sapwood, untreated	21 × 100	14	8.9
Scots pine sapwood, Thermo-D	21 × 100	14	11.2
Scots pine heartwood, untreated	28 × 125	14	11.4
Scots pine heartwood, Thermo-D	28 × 125	14	5.0
Norway spruce sapwood, untreated	21 × 100	14	12.8
Norway spruce sapwood, Thermo-D	21 × 100	14	4.7
Norway spruce heartwood, untreated	28 × 150	14	13.0
Norway spruce heartwood, Thermo-D	28 × 150	14	4.6
WRC	28 × 150	4	9.5
Impregnated Scots pine, CCA (NWPC class A)	28 × 100	7	–
Impregnated Scot pine, CC (NWPC class AB)	28 × 100	7	–

Note: CCA, copper chromium arsenic.

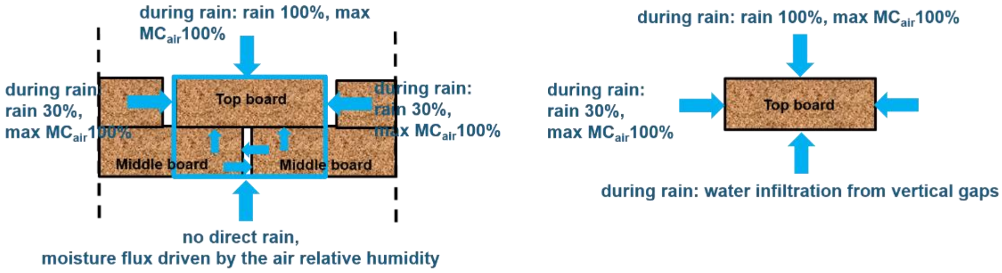

Figure 29 Schemes of the two-layered decking to be used for the modelling. Left: top and middle board model. Right: simplified model for the top board.

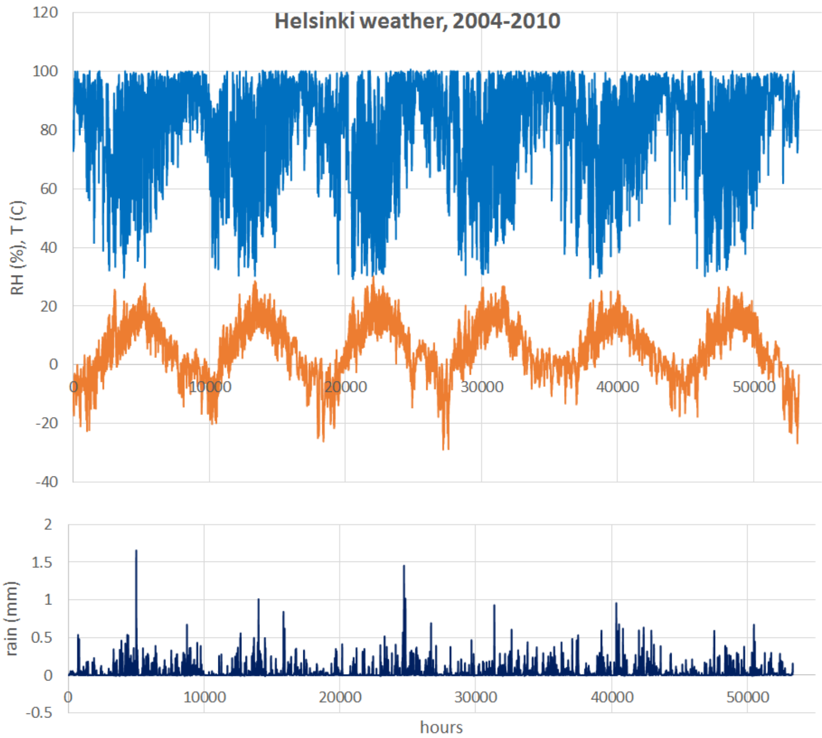

Figure 30 Helsinki weather from 2004 to 2010.

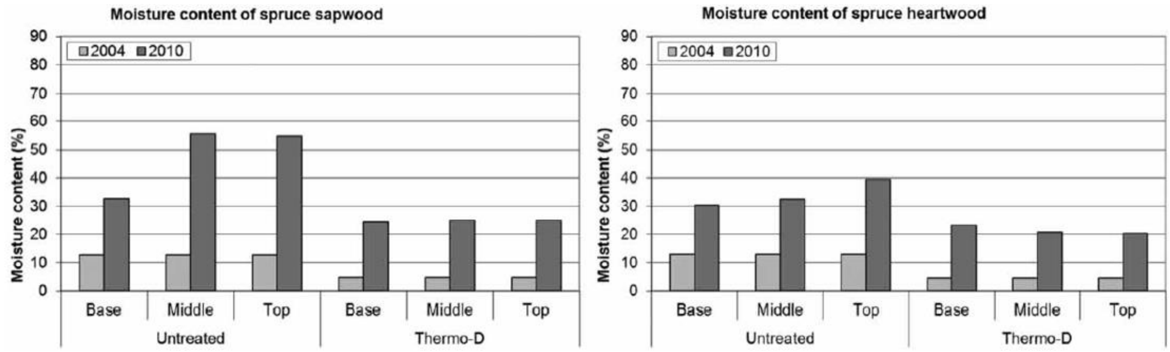

Figure 31 Initial and 6 years moisture content measured in spruce sapwood and hearthwood for the case of untreated wood and Thermowood in the top, middle and base boards of the system.

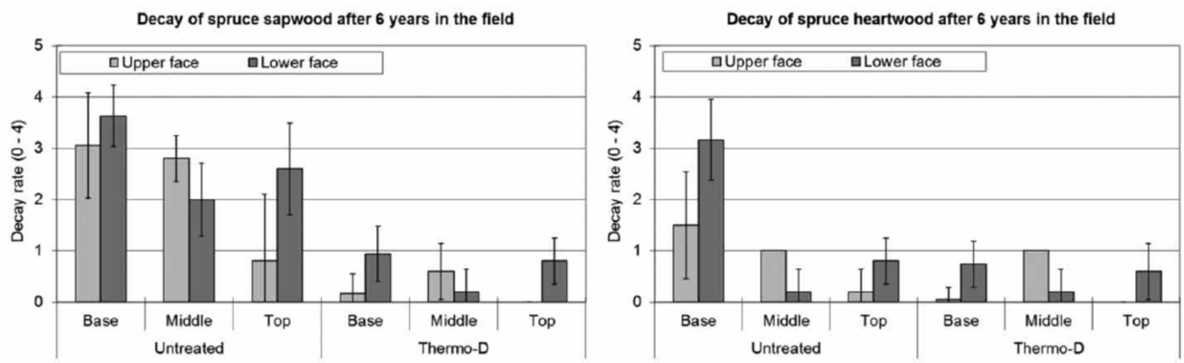

Figure 32 Decay rate in spruce sapwood and hearthwood for the case of untreated wood and Thermowood in the top, middle and base boards of the system after 6 years.

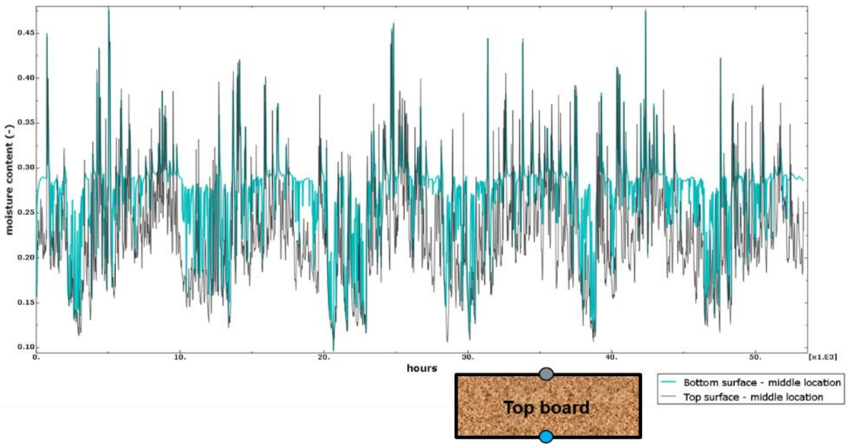

Figure 33 FEM simulation. Moisture content vs time for the cross section of the top board, untreated spruce.

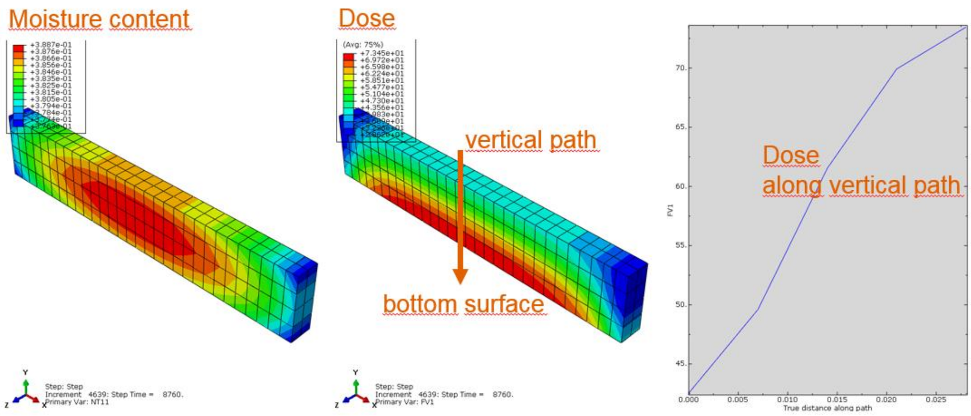

Figure 34 FEM solution for the cross section of the top board, untreated spruce after 1 year. Left: distribution of the moisture content; middle: distribution of the dose; right: dose along the vertical path marked in the middle figure.

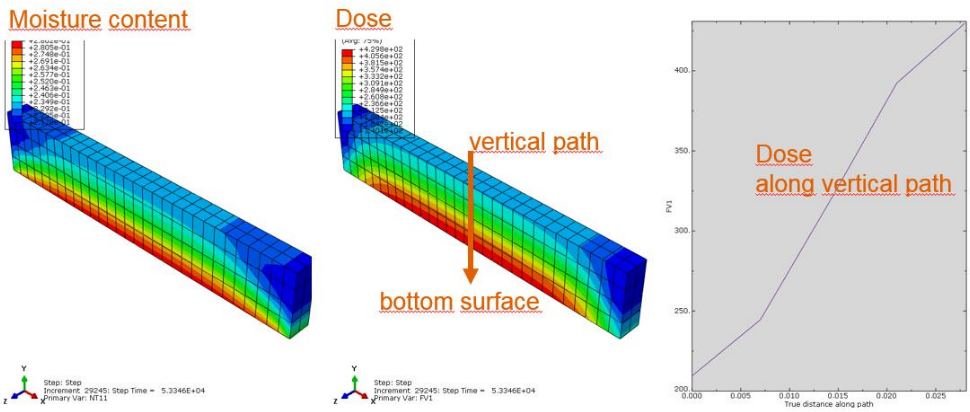

Figure 35 FEM solution for the cross section of the top board, untreated spruce after 6 years. Left: distribution of the moisture content; middle: distribution of the dose; right: dose along the vertical path marked in the middle figure.

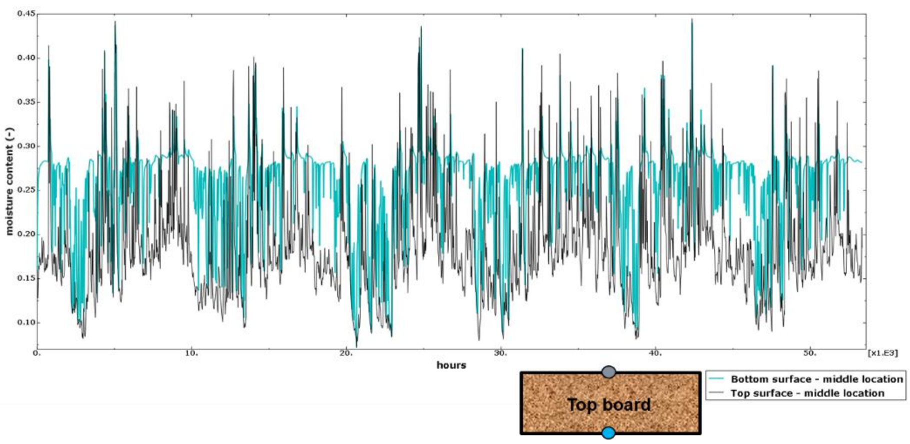

Figure 36 FEM simulation. Moisture content vs time for the cross section of the top board, Thermowood spruce.

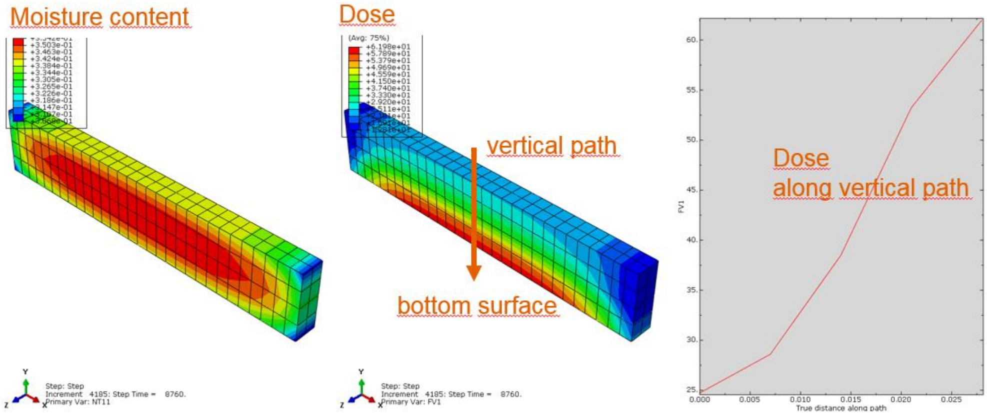

Figure 37 FEM solution for the cross section of the top board, Thermowood spruce after 1 year. Left: distribution of the moisture content; middle: distribution of the dose; right: dose along the vertical path marked in the middle figure.

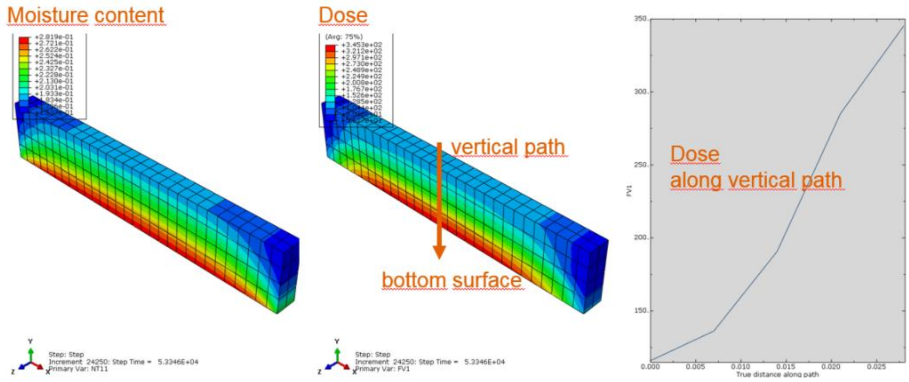

Figure 38 FEM solution for the cross section of the top board, Thermowood spruce after 1 year. Left: distribution of the moisture content; middle: distribution of the dose; right: dose along the vertical path marked in the middle figure.

Table 10. Decay rating for untreated and Thermowood spruce as a function of the dose (Figure 27b)

	decay rating	
	Untreated spruce	Thermowood spruce
1 year	0.2	0.15
6 years	1.5	1.0

10. MEASUREMENTS OF SCRATCH RESISTANCE IN PEG-IMPREGNATED GREEN WOOD

The Digimoist database includes also measurements of scratch resistance in green wood stabilized against water by using the technology of PEG impregnation. Scratch tests (Figure 39) were carried out at VTT in a previous project in collaboration with Uppsala University were the PEG-impregnated samples of green spruce were prepared. During DigiMoist1 project, the results were collected, analysed and published on the peer-reviewed journal Wood Science and Technology (Fortino et al. 2020 https://doi.org/10.1007/s00226-020-01179-0). The scratch test results, quantified in terms of frictional forces and permanent residual depths (Figure 40), reveal that the scratch resistance of wood samples depends on their PEG concentration and density, as well as on the indenter tip size and material, and on the normal force and direction during scratching. Due to the lack of literature on the scratch tests of wood, the results will serve as a scientific reference for future studies on the scratch resistance of untreated or treated dry wood, including also Thermowood, and other wood-based products. The results summarized in Figs. 41 confirm the effect of water stabilisation due to PEG impregnation.

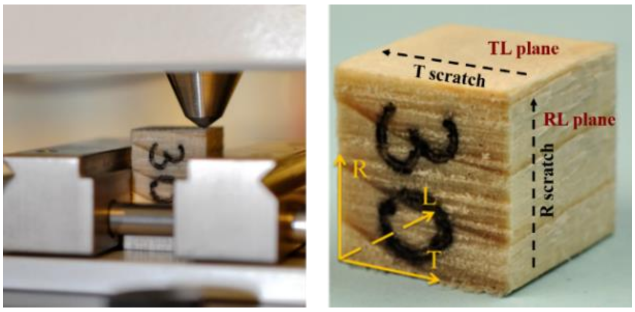

Figure 39 Left: PEG-impregnated sample of Norway spruce under scratch test indenter. Right: radial (R), tangential (T) and longitudinal (L) directions of wood and examples of scratches close to the edges in the T direction (TL plane) and R direction (RL plane).

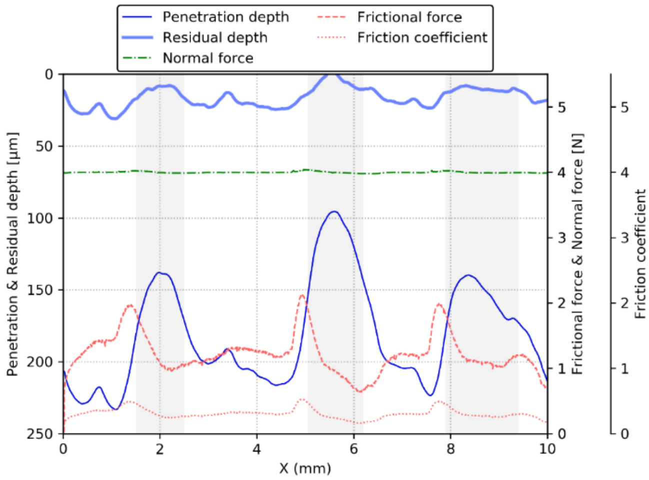

Figure 40. Typical results of the scratch test in the radial direction. The graph shows the normal force [N], residual depth [µm], penetration depth [µm], frictional force [N] and friction coefficient [-] as a function of the scratch length (=10mm). Approximated locations of latewood shaded.

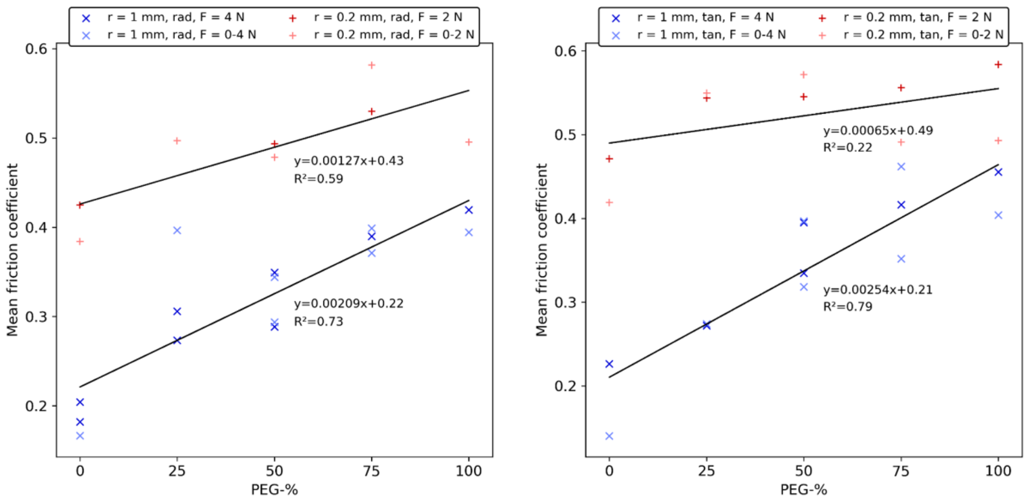

Figure 41. Mean friction coefficient (over all samples) as a function of PEG concentration in radial (rad, RL plane) and tangential (tan, TL plane) scratch directions for all tests. Steel ball indenter (radius r = 1 mm) with constant normal load of 4 N or increasing load from 0 to 4 N, and diamond tip indenter (radius r = 0.2 mm) with constant normal load of 2 N or increasing load from 0 to 2 N were applied in tests.

11. Conclusions

The DigiMoist1 project developed an input database as well as several numerical tools to simulate the hygro-thermal response of wooden components of buildings under different Finnish climates. The project was carried out in collaboration with partners Jartek Invest Oy and Stora Enso, with the ForestValue project Click Design and with other international partners. As a main result of the project, several reference pre-calculations were carried out for various glulam and CLT cross section dimensions. These results, intended as components of the input database of the *DigiMoist toolset*, are available for the funders and partners of DigiMoist1 project in a shared workspace.

Furthermore, a first evaluation of the decay risk, related to the values of wood moisture content above 20-25%, was numerically assessed for boards in untreated spruce and thermally treated spruce (Thermowood, TW) tested in a previous VTT project. For the TW case, a new hygro-thermal model was also proposed by using the experimental measurements carried out by Jartek Oy.

The numerical tools developed within Digimoist1 project can be directly used in future national industrial projects to solve industrial problems related to the hygro-thermal performance of new wooden components or to assist the monitoring and maintenance of existing wooden components of buildings under Finnish climates. Furthermore, the prepared DigiMoist tools can be implemented within the VTT Web Factory open source platform to provide a user-friendly tool to several users in the field of timber engineering.

Acknowledgement

Project DigiMoist1 was funded by the Ministry of the Environment of Finland, which is gratefully acknowledged.

REFERENCES

Berge B. (2009) The ecology of building materials, Architectural Press, Elsevier, Second Edition, 2009.

Björkholtz D. Lämpö ja kosteus, rakennusfysiikka, Rakennustieto Oy, Helsinki 1997.

Brischke C. and Mejer-Veltrup L. (2016) Modelling timber decay caused by brown rot fungi, Materials and Structures 49:3281–3291.

Buss H. Aktuelles Tabellenhandbuch, Feuchte, Wärme, Schall, mit Formeln und Erläuterungen, WEKA Baufachverlage GmbH, 2. Edition, 1994, ISBN 3-8111-3080-3.

Di Blasi C. (1998) Multi-phase moisture transfer in the high-temperature drying of wood particles, Chem. Eng. Sci. 53:53-366.

Droin-Josserand A, Taverdet JM, Vergnaud JM (1989) Modelling the process of moisture adsorption in three dimensions by wood samples of various shapes, Wood Science and Technology 23, pp. 259–271.

Eriksson J., Ormarsson S., Petersson H. (2006) Finite-Element Analysis of Coupled Nonlinear Heat and Moisture Transfer in Wood, Numer. Heat Tr. A-Appl. 50:851-864.

Fortino S., Mirianon F., Toratti T. (2009) A 3D moisture-stress FEM analysis for time dependent problems in timber structures, Mech. Time-Depend. Mater. 13(4): 333–356.

Fortino S., Genoese A., Genoese A., Nunes L., Palma P. (2013) Numerical modelling of the hygro-thermal response of timber bridges during their service life: A monitoring case-study. Constr. Build. Mater. 47 (2013) 1225-1234.

Fortino S., Genoese A., Genoese A., Rautkari L. (2013) FEM simulation of hygro-thermal behaviour of wood under surface densification at high temperature, J. Mater. Sci. 48:7603-7612.

Fortino S., Hradil P., Genoese A., Genoese A., Pousette, A. (2019a) Numerical hygro-thermal analysis of coated wooden bridge members exposed to Northern European climates. Construction and Building Materials, 208:492–505.

Fortino S., Hradil P., Metelli G. (2019b) Moisture-induced stresses in large glulam beams. Case study: Vihantasalmi Bridge, Wood Material Science and Engineering, DOI: 10.1080/17480272.2019.1638828 (2019).

Fortino S., Metsäjoki J., Ronkainen H., Heinemann S., Salminen L.I. (2020) Scratch resistance of PEG-impregnated green wood: a method for evaluation of swollen wood properties. Wood Sci Technol 54**,** 715–735 (2020). https://doi.org/10.1007/s00226-020-01179-0

Fragiacomo M., Fortino S., Tononi D., Usardi I., Toratti T. (2011) Moisture-induced stresses perpendicular to grain in timber sections exposed to European climates. Eng. Struct. 33:3071-3078.

Frandsen H.L. (2007) Selected Constitutive models for simulating the hygromechanical response of wood. Dissertation no. 10, Dep. of Civil Engineering, Aalborg University; ISSN: 1901-7294, 2007.

Frandsen H.L. (2005) Modelling of moisture transport in wood – State of the Art and Analytic Discussion. Wood Science and Timber Engineering, Paper no. 1, 2nd ed., ISSN-1395-7953 R0502, Dept. of Building Technology and Structural Engineering, Aalborg University.

Fredriksson M., Johansson P. (2016) A method for determination of absorption isotherms at high relative humidity levels: measurements on lime-silica brick and Norway spruce (picea abies (l.) karst.). Dry Technol 34:132–141.

Gelin L. "Not in my Building" Moisture and Mold Growth and the Specification of Wallcovering, Technical report, Johns Manville Textra™ Glass Textile Wallcoverings, P. O. Box 5108, Denver, Colorado 80217-5108, www.jm.com/.

Hanhijärvi A. (1995) Modelling of creep deformation mechanisms in wood, Dissertation Helsinki University of Technology, Espoo, Finland.

Hedlin C.P. (1967) Sorption isotherms of twelve woods at subfreezing temperatures, Forest Prod. J. 17(12):43–48.

Hirsch M. (2013) Hygrothermische Simulation von Brettsperrholz. Master Thesis. University of Hamburg.

Häglund M. (2010) Parameter influence on moisture induced eigen-stresses in timbers. Eur J Wood Wood Prod 2010, 68(4):397–406.

Janssen H., Blocken B., Carmeliet J. (2007) Conservative modelling of the moisture and heat transfer in building components under atmospheric excitation, Int. J. Heat Mass Transfer 50:128-1140.

Karagiozis A. N. Importance of Moisture Control in Building Performance. Oak Ridge National Laboratory, Building Technology Center, Oak Ridge, TN, 37831-6070, karagiozisan@ornl.g.

Khang W., Chug W.Y. (2009) Liquid water diffusivity of wood from the capillary pressure–moisture relationJ Wood Sci 55:91–99.

Koponen H. (1984) Dependences of moisture diffusion coefficients of wood and wooden panels on moisture content and wood properties. Paperi ja Puu 12:740–745.

Koponen S. Lämpö- ja kosteusoloiltaan miellyttävä puutalo, vaihe 2, TKK-TRT osatutkimus, Raportti 1, 2002.

Krabbenhøft K. (2003) Moisture Transport in Wood. A Study of Physical--Mathematical Models and their Numerical Implementation. Ph.D. Thesis, Department of Civil Engineering Technical University of Denmark.

Meyer-Veltrup L., Brischke C., Alfredsen G., Humar M., Flæte P-O., Isaksson T., Larsson Brelid P., Westin M., Jermer J. (2017) The combined effect of wetting ability and durability on outdoor performance of wood - development and verification of a new prediction approach. Wood Sci. Technol. 51:615-637.

Metsä-Kortelainen S. & Viitanen H. (2015) Durability of thermally modified sapwood and heartwood of Scots pine and Norway spruce in the modified double layer test, Wood Mater Sci Eng, DOI: 10.1080/17480272.2015.1061596.

Nevander L.E., Elmarsson B. Fukthandbok, Praktik och teori, AB Svensk Byggtjänst, 1994 Stocholm, 2. Edition, ISBN 91-7332-716-6.

Niklewski J., Fredriksson M., Isaksson T. (2016) Moisture content prediction of rain-exposed wood: Test and evaluation of a simple numerical model for durability applications, Build. Environ. 97:126-136.

Nilsson L.-O. (1988) "Moisture transport properties of wood and wood-based boards – an inventory and analysis of knowledge and required knowledge" (in Swedish), Report P-88:4, dept. Of building materials, Chalmers University of Technology, Göteborg, Sweden.

Trcala M. (2012) A 3D transient nonlinear modelling of coupled heat, mass and deformation fields in anisotropic material, Int. J. Heat Mass Transfer 55:4588-4596.

Pang, S. (1997) Relationship between a diffusion model and a transport model for softwood drying', Wood and Fiber Science, 29(1):58–67.

Perré P. Turner I.W. (1999) A 3-D version of TransPore: a comprehensive heat and mass transfer computational model for simulating the drying of porous media, Int. J. Heat Mass Transfer 42:4501-4521.

Perré, P. and Turner I.W. (2001) Determination of the Material Property Variations Across the Growth Ring of Softwood for Use in a Heterogeneous Drying Model - Part 1 Capillary Pressure, Tracheid Model and Absolute Permeability. Holzforschung 55(3):pp. 318-323.

Rode C., Clorius C.O. (2004) Modeling of moisture transport in wood with hysteresis and temperature-dependent sorption characteristics, in: Proceedings of the Conference Performance of Exterior Envelopes of Whole Building IX. Sheraton Sand Key Resort, Clearwater Beach, Florida, 2004 ASHRAE, pp. 1–15.

Sjödin, J. (2006) Steel-to-timber dowel joints—influence of moisture induced stresses. Licentiate Thesis, Växjö University.

The Engineering Tool Box, Moisture Transport through Building Walls and Roofs, http://www.engineeringtoolbox.com/

Engelund Thybring E., Kymäläinen M, Rautkari L. (2017) Experimental techniques for characterising water in wood covering the range from dry to fully watersaturated. Wood Sci Technol https://doi.org/10.1007/s00226-017-0977-7

Tikkurila Oy, 2002. Values of permeance and resistance given by the paint producer.

Younsi R., Kocaefe D., Poncsak S., Kocaefe Y. (2007) Computational modelling of heat and mass transfer during the high-temperature heat treatment of wood, Appl. Therm. Eng. 27:1424-1431.

WUFI https://wufi.de/en/

Zarr R., Burch D., Fanney A. Heat and Moisture transfer in Wood-Based Wall Construction: Measured versus Prediction. NIST Building Science Series 173, 1995.

APPENDIX A – COATING PERMEANCE AND RESISTANCE

Review by Simo Koponen, 2002

Material/paint type and substrate	Dry/Wet cup method	Resistance m2 s Pa/kg	Permeance kg/m2 s Pa	Substrate	Reference
Pressure polymer paint, Novaplast 2	W	2,3E+07	4,3E-08		Tikkurila (2002)
Paper wallpaper		1,4E+08	7,4E-09		Nevander (1994)
Glue paint		1,6...2,2E+8	4,5...6,3E-9		Buss (1994)
Wallpaper		3,0E+08	3,3E-09		The Engineering Tool Book https://www.engineeringtoolbox.com/moisture-transport-walls-d_163.html
Akrylic copolymer paint, Siroplast 20	W	3,7E+08	2,7E-09	permeable film	Tikkurila (2002)
½" Gypsum wall board (=GWB), no paint	D	4,2...4,6E+8	2,2...2,4E-9		Gelin L. https://www.jm.com/
Water-based acrylic varnish Paneeli-Ässä	W	5,5E+08	1,8E-09	permeable film	Tikkurila (2002)
Pressure polymer paint, Novaplast 20	W	5,7E+08	1,7E-09	permeable film	Tikkurila (2002)
Pressure polymer paint, Novaplast 7	W	5,8E+08	1,7E-09	permeable film	Tikkurila (2002)
Acryl latex paint 50 µm,	RH 90%	6,8E+08	1,5E-09		Nevander (1994)

no primer					
Silicate paint 80µm		7,0E+08	1,4E-09		Björkholtz (1997)
Acryl latex paint, Harmony	W	7,9E+08	1,3E-09	Permeable film	Tikkurila (2002)
Acrylic latex paint, Remontti-Ässä	W	8,0E+08	1,3E-09	Permeable film	Tikkurila (2002)
Silicate paint 100µm		8,0E+08	1,3E-09		Björkholtz (1997)
Interior latex paint system = primer +finish coat	D/W	1,0E+09	1,0E+09	gypsum wallboard	Zarr et al. (1995)
PVA latex paint 100µm		1,0E+09	1,0E+09		Björkholtz (1997)
½" GWB with JM Textra + 2 coats flat paint*	D	1,1E+09	9,4E-10	gypsum wallboard	Gelin L. https://www.jm.com/
Vinyl Wallpaper		1,4E+09	7,4E-10		Nevander (1994)
PVA latex paint 120µm		1,4E+09	7,1E-10		Björkholtz (1997)
Latex Primer		1,75...2,5 E+09	4,0...5,7 E-10		Gelin L. https://www.jm.com/
Latex and primer		2,2E+09	4,5E-10	gypsum wallboard	Karagiozisan A.N., karagiozisan@ornl.g
½" GWB + latex Primer	D	1,94...2,5 E+09	4,0...5,1 E-10	gypsum wallboard	Gelin L. https://www.jm.com/
Latex and primer		2,5E+09	4,0E-10		Karagiozisan A.N., karagiozisan@ornl.g
Acryl latex paint 100µm		2,5E+09	4,0E-10		Björkholtz (1997)
Acryl latex paint 50 µm, no primer	RH 60%	2,7E+09	3,7E-10		Nevander (1994)

Teknos Aqua Grund Cyppress		3,1E+09	3,2E-10		Koponen (2002)
Alkyd oil paint 50 µm, no primer	RH 90%	3,4E+09	3,0E-10		Nevander (1994)
Paint for walls, matt		2,0...5,0E+09	0,2...5,0E-10		The Engineering Tool Book https://www.engineeringtoolbox.com/moisture-transport-walls-d_163.html
½" GWB with JM Textra (glass tectile wallcovering) + 2 coats satin paint	D	3,6E+09	2,8E-10	gypsum wallboard	Gelin L. https://www.jm.com/
Water-based epoxy, Akvacoat 100"new"	W	3,9E+09	2,6E-10	permeable film	Tikkurila (2002)
Acryl latex paint 200µm		4,0E+09	2,5E-10		Björkholtz (1997)
Chlorinated rubber paint 40µm		4,7E+09	2,1E-10		Björkholtz (1997)
PVC paint 30µm		6,0E+09	1,7E-10		Björkholtz (1997)
½" GWB with JM Textra, latex primer + 2 coats satin paint*	D	6,7E+09	1,5E-10	gypsum wallboard	Gelin L. https://www.jm.com/
Alkyd paint, Pesto	W	7,8E+09	1,3E-10	permeable film	Tikkurila (2002)
Chlorinated rubber paint 50µm		8,0E+09	1,3E-10		Björkholtz (1997)
PVC paint 40µm		9,0E+09	1,1E-10		Björkholtz (1997)
Alkyd paint 90µm		9,5E+09	1,1E-10		Björkholtz (1997)

Oil paint		5,4...14E+09	0,7...1,9E-10		Buss (1994)
Oil paint		1,0E+10	1,0E+10		The Engineering Tool Book https://www.engineeringtoolbox.com/moisture-transport-walls-d_163.html
Alkyd oil paint 50 µm, no primer	RH 60%	1,0E+10	9,9E-11		Nevander (1994)
Polyurethane paint 30µm		1,2E+10	8,7E-11		Björkholtz (1997)
Oil lacquer		1,1...1,6E+10	6,2...9,1E-11		Buss (1994)
Alkyd paint 120µm		1,6E+10	6,3E-11		Björkholtz (1997)
Polyurethane paint 30µm		1,6E+10	6,3E-11		Björkholtz (1997)
PVC lacquer		1,4...2,8E+10	3,6...7,1E-11		Buss (1994)
Chlorinated rubber paint TEMACOAT RM40	W	2,7E+10	3,7E-11	permeable film	Tikkurila (2002)
Chlorinated rubber lacquer		1,4...4,5E+10	2,2...7,1E-11		Buss (1994)
Alkyd paint		2,0...4,0E+10	2,5...5,0E-11		The Engineering Tool Book https://www.engineeringtoolbox.com/moisture-transport-walls-d_163.html
Moisture barrier, Lujamethodks+2xLujapk	W	3,4E+10	3,0E-11	permeable film	Tikkurila (2002)
½" GWB + Vinyl Wallcovering	D	2,2...35E+10	2,9E-12	gypsum wallboard	Gelin L. https://www.jm.com/

APPENDIX B – MOISTURE GRADIENT AND MOISTURE CONTENT CONTOURS IN FINLAND

Glulam 60 mm – Middle lamella – Uncoated

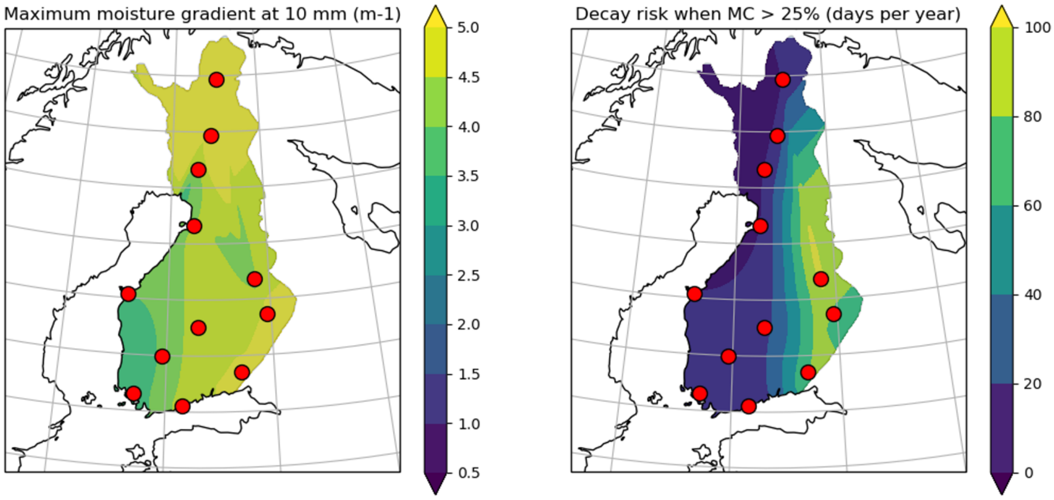

Glulam 60 mm – Middle lamella – Weak coating

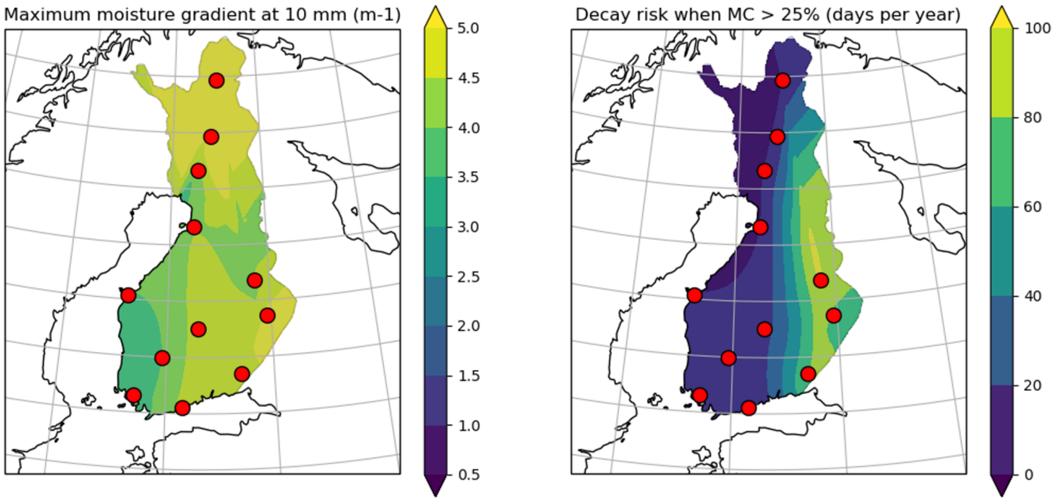

Glulam 60 mm – Middle lamella – Standard coating

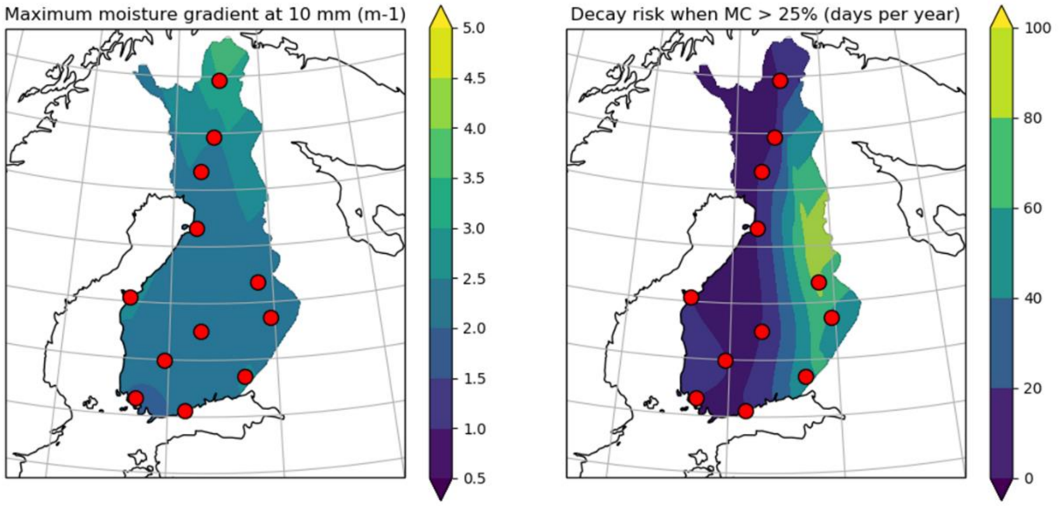

Glulam 60 mm – Middle lamella – Strong coating

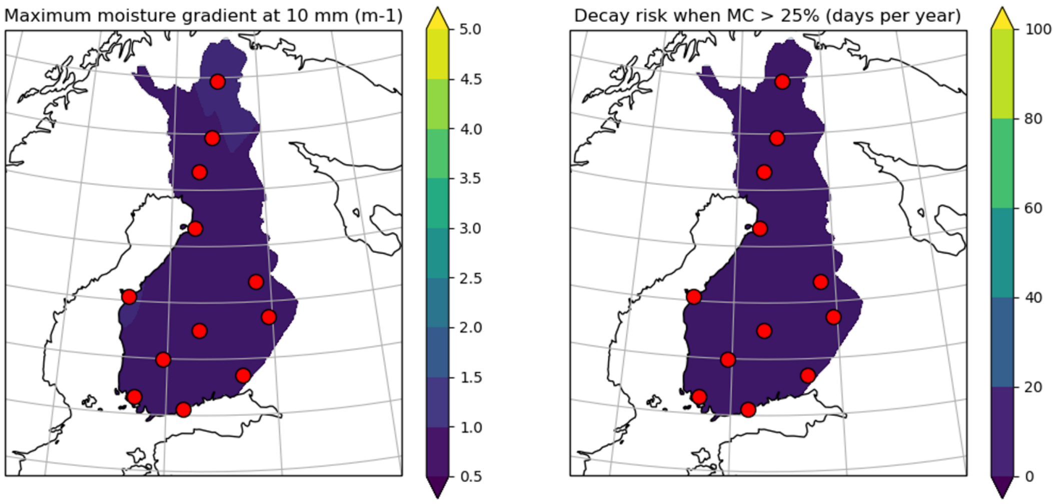

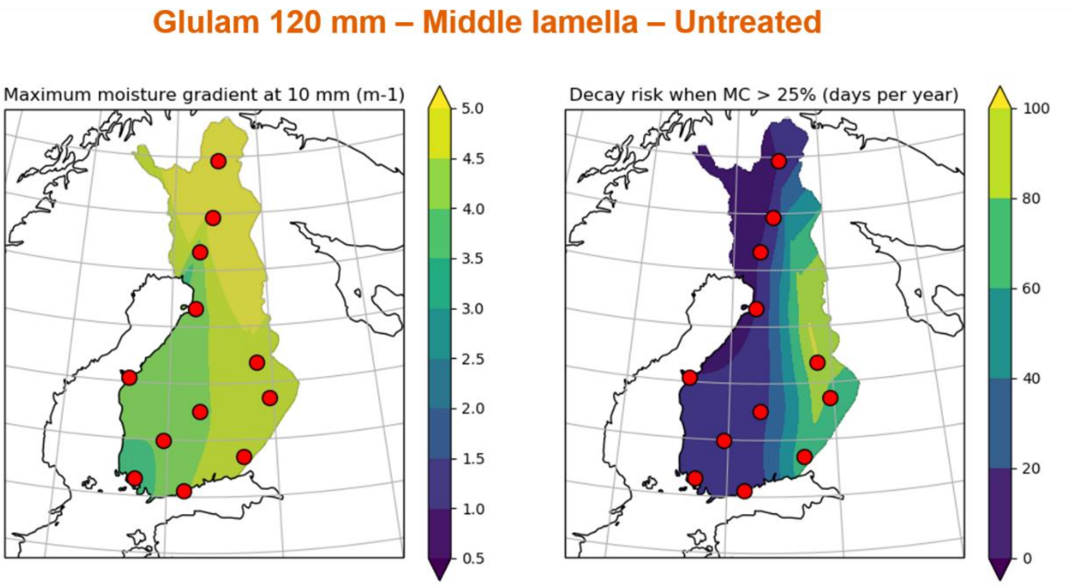
Glulam 120 mm – Middle lamella – Untreated
Maximum moisture gradient at 10 mm (m-1)
5.0
4.5
4.0
3.5
3.0
2.5
2.0
1.5
1.0
0.5
Decay risk when MC > 25% (days per year)
100
80
60
40
20
0

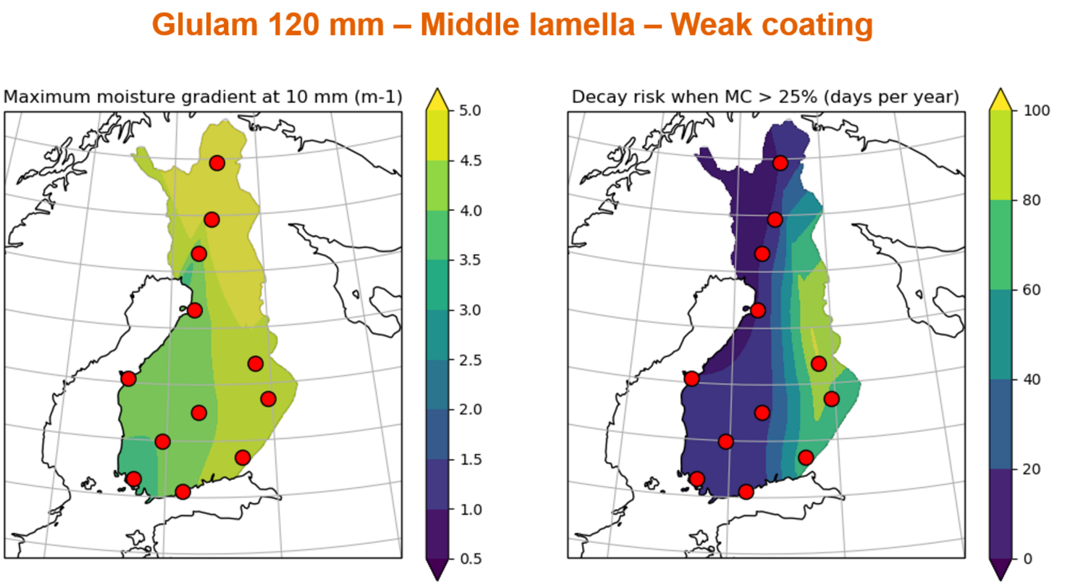
Glulam 120 mm – Middle lamella – Weak coating
Maximum moisture gradient at 10 mm (m-1)
5.0
4.5
4.0
3.5
3.0
2.5
2.0
1.5
1.0
0.5
Decay risk when MC > 25% (days per year)
100
80
60
40
20
0

Glulam 120 mm – Middle lamella – Standard coating

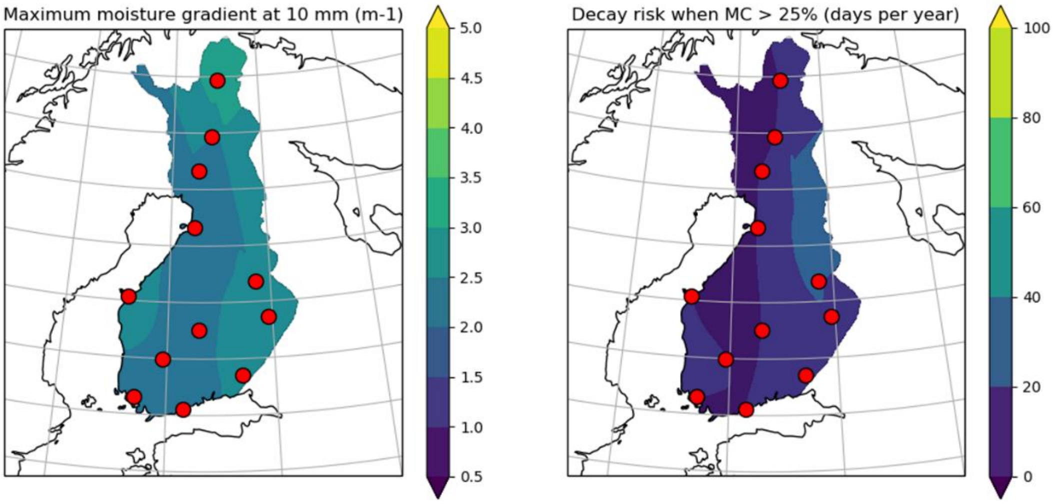

Glulam 120 mm – Middle lamella – Strong coating

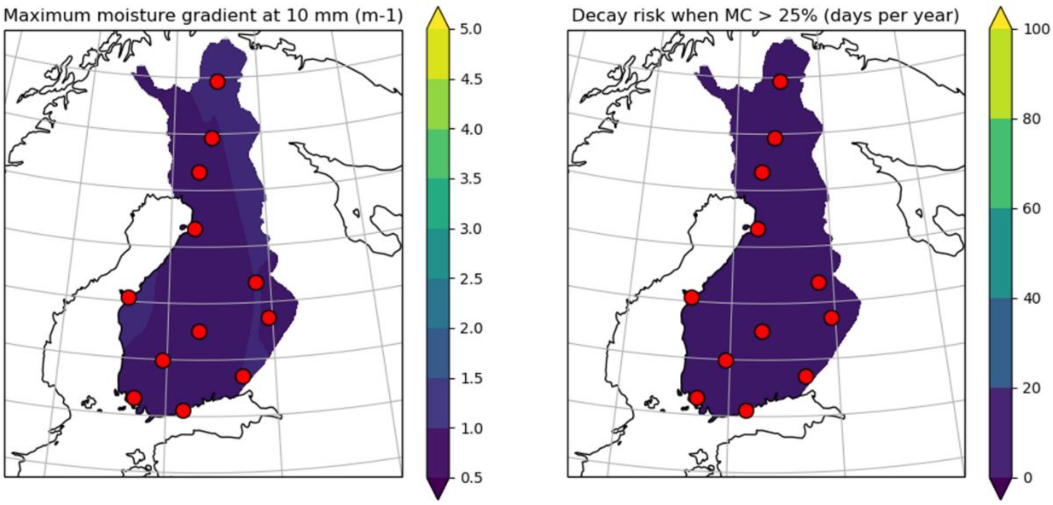

Glulam 200 mm – Middle lamella – Weak coating

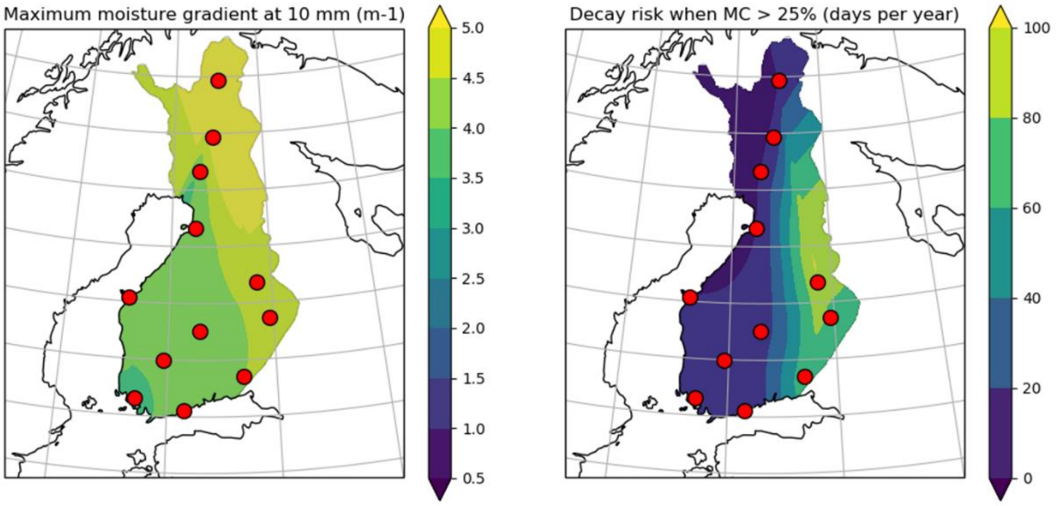

Glulam 200 mm – Middle lamella – Uncoated

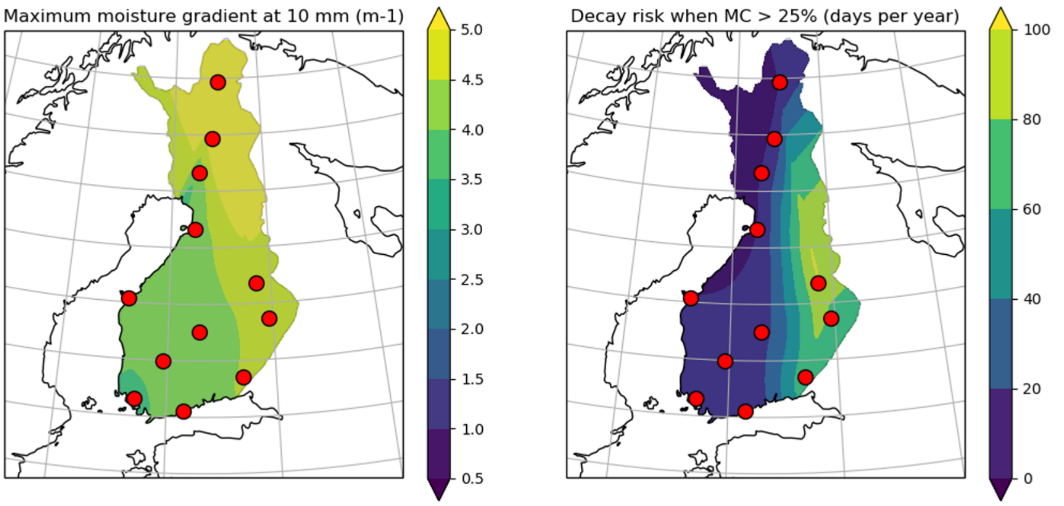

Glulam 200 mm – Middle lamella – Standard coating

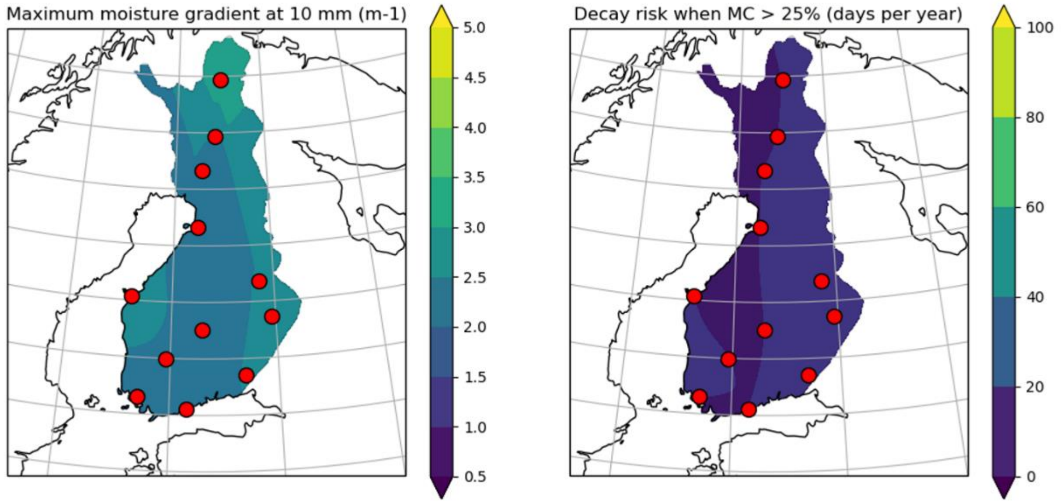

Glulam 200 mm – Middle lamella – Strong coating

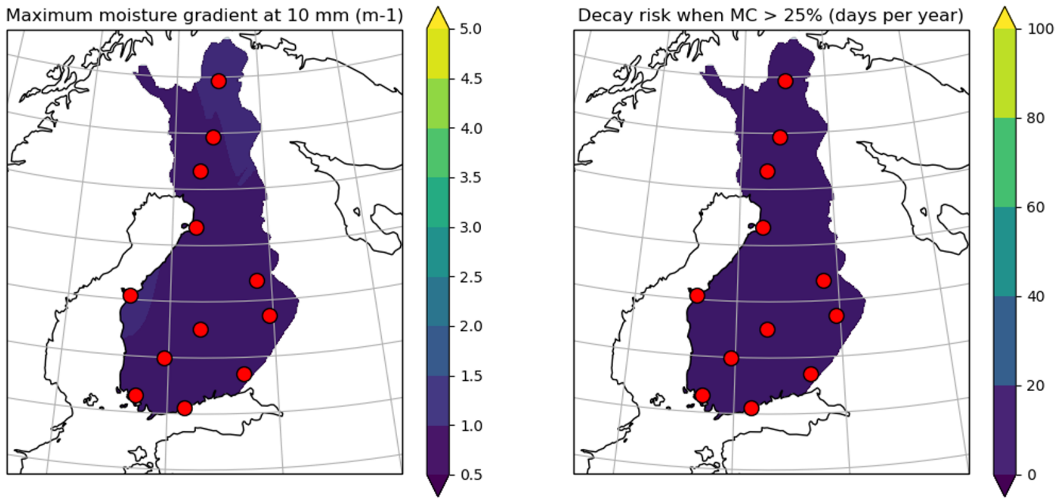

CLT 3S – 60 mm – Uncoated

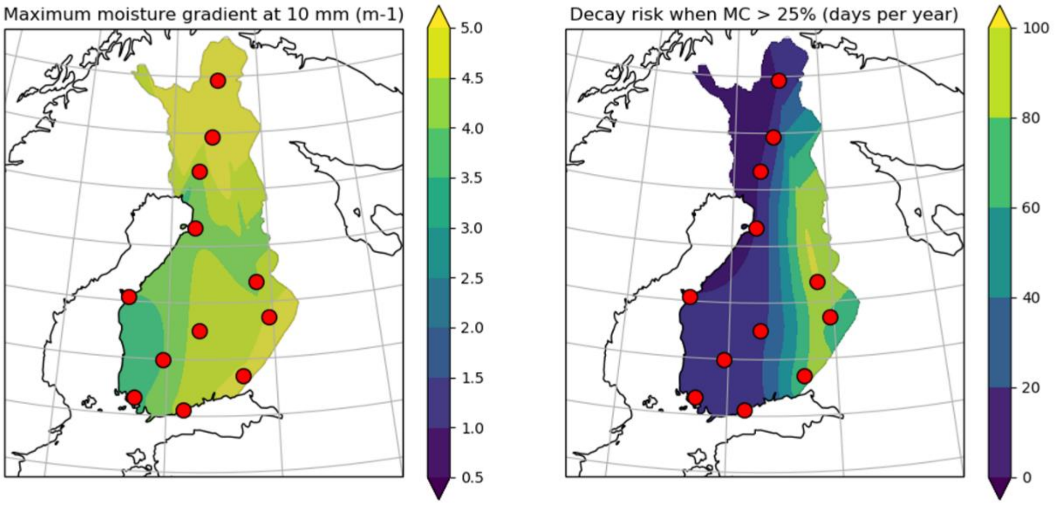

CLT 3S – 60 mm – Weak coating

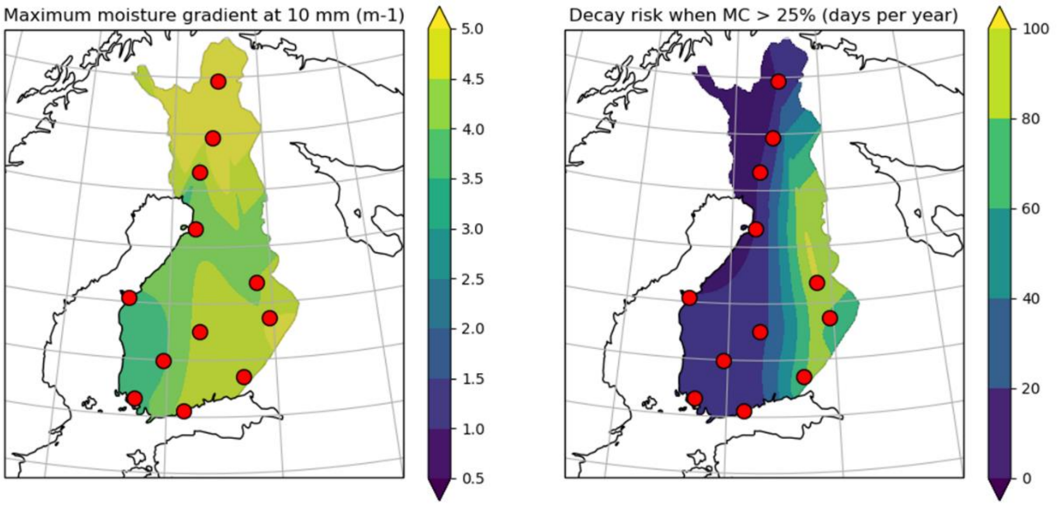

CLT 3S – 60 mm – Standard coating

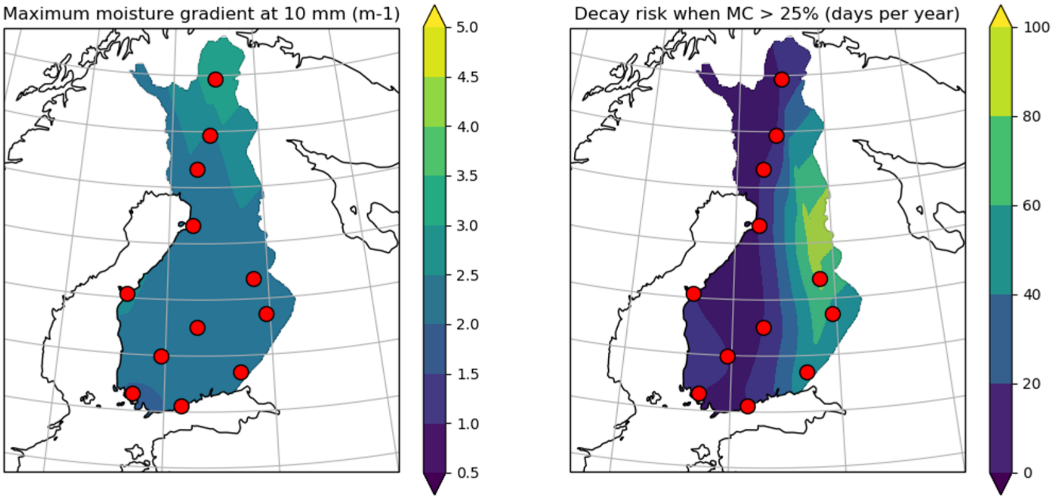

CLT 3S – 60 mm – Strong coating

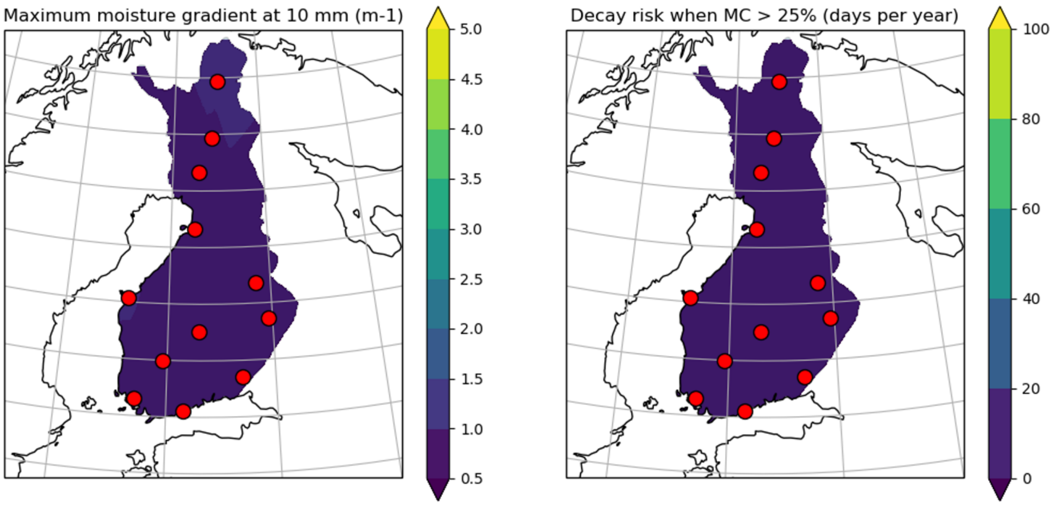

CLT 5S – 100 mm – Uncoated

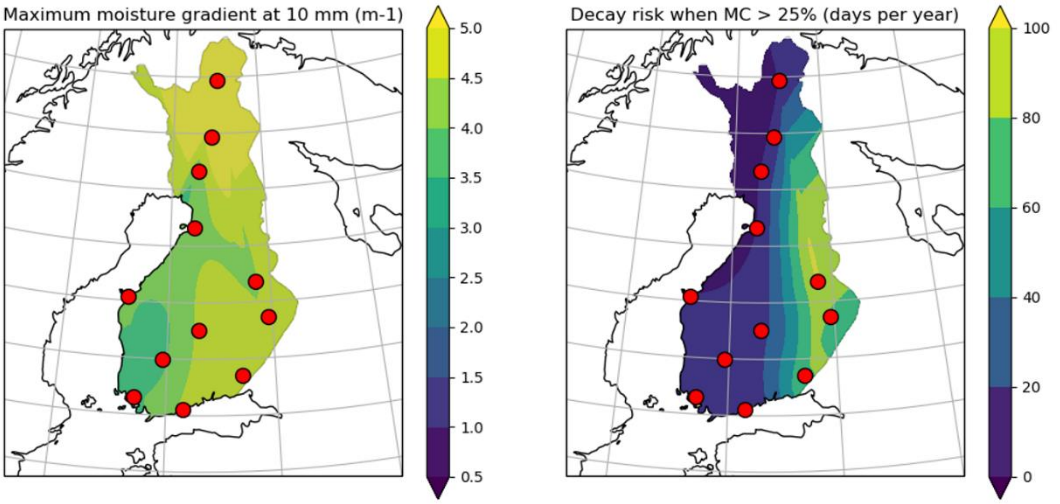

CLT 5S – 100 mm – Weak coating

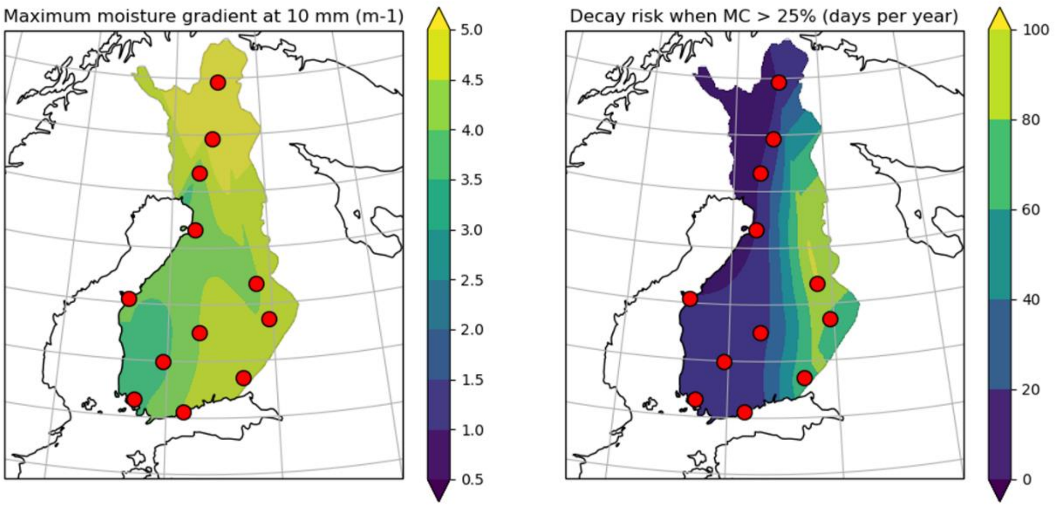

CLT 5S – 100 mm – Standard coating

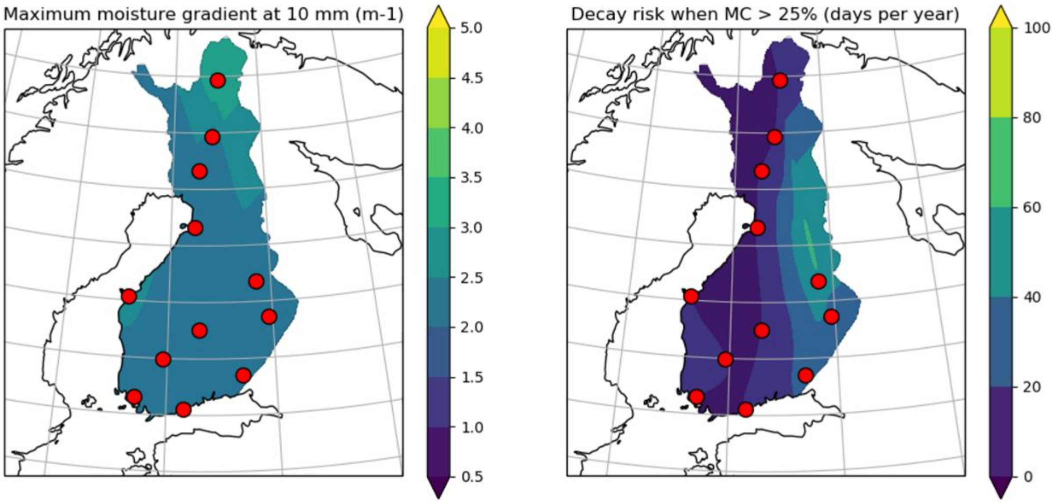

CLT 5S – 100 mm – Strong coating